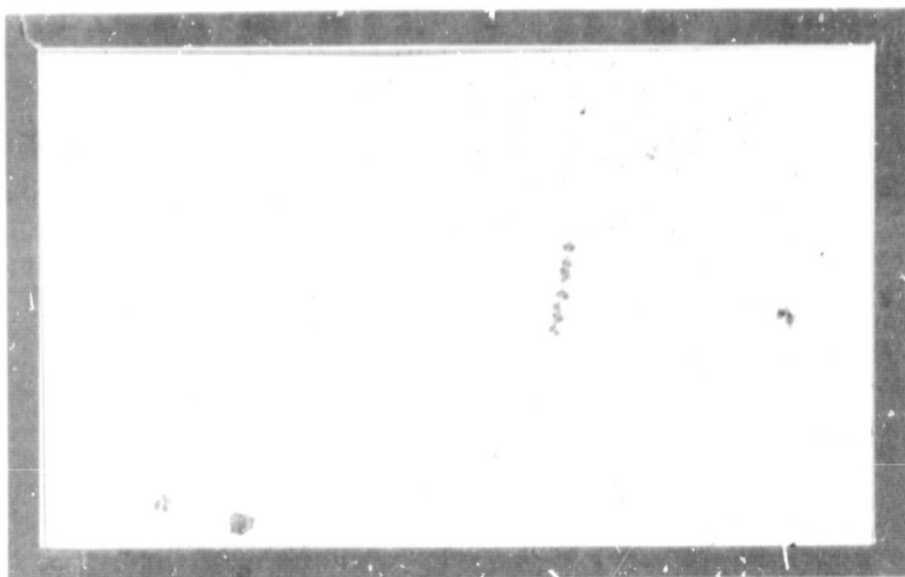


## **General Disclaimer**

### **One or more of the Following Statements may affect this Document**

- This document has been reproduced from the best copy furnished by the organizational source. It is being released in the interest of making available as much information as possible.
- This document may contain data, which exceeds the sheet parameters. It was furnished in this condition by the organizational source and is the best copy available.
- This document may contain tone-on-tone or color graphs, charts and/or pictures, which have been reproduced in black and white.
- This document is paginated as submitted by the original source.
- Portions of this document are not fully legible due to the historical nature of some of the material. However, it is the best reproduction available from the original submission.



(NASA-CR-173969) MATERIALS FOR  
HIGH-TEMPERATURE THERMOELECTRIC CONVERSION  
Annual Technical Report (Stanford Univ.)  
59 p HC A04/MF A01

N84-34011

CSSL 10A

Unclas

G3/44 01077



CENTER FOR MATERIALS RESEARCH

STANFORD UNIVERSITY • STANFORD, CALIFORNIA

Center for Materials Research  
McCullough Building  
Stanford University  
Stanford, CA 94305

Annual Technical Report  
on  
MATERIALS FOR HIGH-TEMPERATURE  
THERMOELECTRIC CONVERSION  
NASA Contract # NAGW-268  
Submitted to  
National Aeronautics and Space Administration  
CMR-P-84-3  
April 1984

Submitted by  
The Board of Trustees of  
The Leland Stanford Jr. University  
Stanford, California 94305

Principal Investigator:

Professor R. S. Feigelson  
Center for Materials Research  
Department of Materials Science &  
Engineering

Associate Investigators:

Dr. D. Elwell  
Center for Materials Research

Professor B. Auld  
Hansen Laboratories

## I. INTRODUCTION

The main aim of this investigation is to develop materials for high temperature thermoelectric energy conversion devices. A major goal of our program is the development of new criteria for the selection of materials, based on a better understanding of the fundamental principles governing the behavior of high-temperature thermoelectric materials. Our experimental program mainly involves the synthesis and characterization of promising new materials and the growth of single crystals so that possible problems associated with grain boundaries and other defects in polycrystalline materials can be eliminated.

## II. DEVELOPMENT OF A PREDICTIVE METHODOLOGY

In our original proposal, three approaches to the development of improved criteria for the selection of new refractory thermoelectric materials were proposed:

- a. Consideration of Fundamentals
- b. Extrapolation from Known Materials
- c. Development of an Alternative "Figure of Merit"

These headings will be used to describe recent findings.

### A. FUNDAMENTALS

#### 1. The Figure of Merit Z:

The maximum efficiency of thermoelectric energy conversion for given hot and cold junction temperatures  $T_H$  and  $T_C$  is given by

$$\eta = \frac{(1 + ZT_M)^{1/2} - 1}{(1 + ZT_M)^{1/2} + T_C/T_H} \cdot \frac{(T_H - T_C)}{T_H} \quad (1)$$

where  $T_M = \frac{1}{2}(T_H + T_C)$  and  $Z = \alpha^2 \sigma / \lambda$ . So the efficiency depends on the figure of merit  $Z$  and therefore on the Seebeck coefficient  $\alpha$ , electrical conductivity  $\sigma$  and thermal conductivity  $\lambda$ . If  $Z = 1 \times 10^{-3}$ ,  $T_C = 800\text{K}$  and  $T_H = 1500\text{K}$ , then  $\eta = 12.5\%$  which would be considered a very acceptable efficiency. A target figure of  $\bar{Z} = ZT = 1$  is considered a desirable goal for both an n- and a p-type material.

Metallic conductors usually have too low Seebeck coefficients for this target to be realistic, and insulators have too low an electrical conductivity, so semiconductors are considered the most appropriate class of materials. Except for silicon carbide, there has been very little research effort to identify promising refractory semiconductors for alternative applications e.g. high-temperature transistors.

The value of  $\alpha$  is small for intrinsic semiconductors since electrons and holes contribute oppositely (i.e. algebraically), and so the requirement that conduction is dominated by a single carrier type at temperatures up to about 1200°C requires a band gap of about 1-2 eV at this temperature. The essential requirements for a high temperature thermoelectric material are therefore a melting point above about 1500°C, a low vapor pressure at the temperature of operation, and a fairly wide bandgap.

Assuming single carrier conduction, the Seebeck coefficient is given by

$$\alpha = \pm k/e[A + \ln(N/n)] \quad (2)$$

for broad band semiconductors, where  $k$  is Boltzmann's constant and  $e$  the electron charge. The  $A$  term represents the kinetic energy transported by the carriers (which depends on the type of scattering), and  $n$  is the carrier concentration with  $N$  the density of states. Usually  $A$  is roughly independent of temperature and so  $\alpha$  decreases with increase of temperature because of the second term in Eq. 2.

If the material is a narrow band semiconductor, with carrier mobility so low that the carriers are small polarons, the first term may increase linearly with temperature because of the energy transported by carriers in hopping to inequivalent sites. This type of behavior can give rise to relatively large values of  $\alpha$  at high temperatures but is associated with a low carrier mobility, hence a low value of  $\sigma$ , especially at relatively low temperatures.

The bandgap of semiconductors is known to decrease with increasing molecular weight and to increase with ionicity of the material. As examples, silicon has a room temperature bandgap of about 1.2 eV while the value for germanium is about half this value.

Gallium phosphide, with a slightly higher molecular weight than germanium, has a bandgap of 2.3 eV and that of zinc sulfide is 3.7 eV. These trends can be used to predict the bandgap in cases where measurements have not been made but where data exists on related materials.

For a chosen material, an optimum doping concentration can usually be calculated to optimize  $\alpha^2\sigma$ , provided that a model which can describe these parameters (e.g. small polaron, wide band with ionized impurity scattering) is available. This optimum concentration is normally in the range  $10^{19}$ - $10^{21}$   $\text{cm}^{-3}$  and is therefore much higher than in conventional semiconductors.

Thermal conductivity has been reviewed by Spitzer (1) and Slack (2). Spitzer stresses the importance of chemical bonding and notes that the lattice contribution to the thermal conductivity ( $\lambda_L$ ) decreases with mean atomic weight, ionicity, coordination number, in defect structures compared with relatively perfect lattices and in ternary materials in comparison with similar binary compounds. As examples of the latter effect, the room temperature thermal conductivity of  $\text{TlBiTe}_2$  is 12 mW/cm deg compared with 29 mW/cm deg for  $\text{TlTe}$ , and that of  $\text{AgTlS}$  is 4.5 mW/cm deg compared with 9 mW/cm deg for  $\text{Ag}_2\text{S}$ . This approach of using a ternary material by appropriate substitution into a binary has already been used extensively and is likely to be an important factor in this current program. Our approach to optimizing the location of chosen dopants will be described later in this report.

Slack (2) gives expressions for the Debye temperature for various types of lattice and obtains good agreement between theoretical and experimental values of  $\lambda$  for adamantane and other simple structures. He stressed the importance of the complexity of the unit cell as a factor which will reduce  $\lambda_L$ . This explains why the thermal conductivity of  $\text{YB}_{68}$  (402 atoms/unit cell) should be lower than that of  $\beta$ -boron (105 atoms/unit cell) which in turn should be lower than that of  $\alpha$ -boron (12 atoms/unit cell). It is this factor which gives substituted  $\beta$ -boron an advantage over materials with the  $\alpha$ -boron type structure ( $\text{B}_4\text{C}$  etc.), provided that the electrical properties of the

former material can be improved by choice of a suitable dopant. The alternative strategy for the production of a material of acceptable figure of merit is to lower the thermal conductivity of a composition having the  $B_4C$  structure, again by appropriate alloying.

## 2. Trends in Families of Materials:

A popular approach often used successfully in the choice of materials for a particular application involves reviewing data tables to make a preliminary selection of materials for detailed literature searches. This approach can be used either to find promising new host lattices for high temperature thermoelectric applications, or to suggest dopants for known materials. In this section we consider some generalizations regarding families of refractory materials, the aim being to identify candidates for further study as alternatives to the materials currently under investigation.

a. Silicides: The relatively high melting point silicides are formed from rare earth, actinide, and the transition metals of the iron, palladium and platinum groups. Their properties are generally similar to those of the borides but the Si-Si bond radius is much larger (1.17- 1.34 Å). The bonding in the lower (metal rich) silicides is essentially metallic, but the Si-Si bonds tend to become increasingly covalent in the higher silicides. Some di- and trisilicides  $MSi_2$  and  $MSi_3$  exhibit semiconducting properties, and higher silicides ( $MSi_4$  etc.) are unknown.

As the M:Si ratio increases the bonding changes from one with isolated Si atoms bonded to metals only (e.g.  $Cr_3Si$ ,  $FeSi$ ), or pairs of atoms, still isolated ( $U_3Si_2$ ) to one-dimensional chains of Si atoms (e.g.  $Mn_3Si_2$ ), two-dimensional layers of Si and metal atoms ( $MoSi_2$ ,  $TiSi_2$ ) or a three-dimensional Si framework ( $ThSi_2$ , rare earth disilicides). Most silicides have very high electrical conductivities, often higher than that of the pure metal. For example,  $WSi_2$  has a room temperature conductivity of  $8 \times 10^4$  (ohm.cm)<sup>-1</sup>. Of the known semiconductors,  $ReSi_2$  has a bandgap of 0.13 eV,  $OsSi_2$  about 1.8 eV (3),  $\beta$ - $FeSi_2$  0.88 eV,  $BaSi$  1.3 eV and  $CrSi_2$  also 1.3 eV. Materials which have already been investigated for

possible thermoelectric applications include  $\text{CrSi}_2$  and  $\text{CoSi}$  (4). The Seebeck coefficient of a sample of  $\text{CrSi}_2$  was from +100 to 150  $\mu\text{V}/\text{deg}$  in the range 300-1000 K, the thermal conductivity 65  $\text{mW}/\text{cm deg}$  and the melting point 1550°C. The  $\text{CoSi}$  was said to be an n-type semiconductor, with  $\alpha$  around -85  $\mu\text{V}/\text{deg}$ ,  $\lambda = 94 \text{ mW}/\text{cm deg}$  and melting point 1460°C. Manganese silicides were investigated by Bienert and Gillen (5) and the best figure of merit was obtained with  $\text{Mn}_4\text{Si}_7$ . The peak value of Z was around  $0.6 \times 10^{-3} \text{K}^{-1}$  at 700K ( $\alpha = 240 \mu\text{V}/\text{deg}$ ;  $\rho \sim 3 \times 10^{-3} \text{ ohm cm}$ ;  $\lambda = 30 \text{ mW}/\text{cm deg}$ ), and Re doping increased this figure to  $0.87 \times 10^{-3} \text{K}^{-1}$ . The maximum operating temperature was stated to be 1150K, although it is not clear from the patent whether there is significant deterioration at this temperature. The phases  $\text{Mn}_5\text{Si}_3$  and  $\text{MnSi}$  have melting points of 1280°C and 1275°C respectively so it is unlikely that the  $\text{Mn}_4\text{Si}_7$  phase will be stable at temperatures around 1200°C. Silicides generally appear worthy of further study.

b. Carbides: Carbides include the most refractory materials known, and many are chemically inert with low vapor pressures. Alkali metal- and alkaline earth carbides hydrolyze readily, as does aluminum carbide. Silicon carbide is a semiconductor with high carrier mobility, which can be made p- and n-type, and has been the subject of intensive investigation for electronic devices operating at high temperature. Its major problem is its high thermal conductivity,  $> 100 \text{ mW}/\text{cm deg}$ , and the equivalent germanium compound is not known so a (Si,Ge)C material of low thermal conductivity is unlikely. Most transition metal, rare earth and refractory metal carbides have metallic conductivity and the only other carbide which looks worthy of further investigation is YC, which is reported to have a room temperature electrical conductivity of  $22 (\text{ohm cm})^{-1}$ .

c. Nitrides: Many transition metals, rare earths and some light elements (Be, B, Al, Si) form refractory nitrides. Their melting points are generally high but they have a greater tendency to dissociate than oxides or sulfides. It is this factor which mainly limits their application in high vacuum devices except at rather low temperatures. The nitrides which have low vapor pressure e.g. TiN, ZrN and NbN, are metallic conductors so nitrides in general are not

very appealing. Boron nitride is exceptional in that it has a low electrical conductivity and low vapor pressure, and it is conceivable that semiconducting compounds could be made, for example by replacing  $C_2$  by BN in carbides.

d. Phosphides: Refractory phosphides are known, e.g. BP, but like nitrides have relatively high vapor pressures. AlP and GaP are semiconductors with high mobilities, but their strong tendency to dissociate is a very serious adverse factor. BP can be made both n- and p-type, with a figure of merit increasing from around  $0.3 \times 10^{-3} K^{-1}$  at  $300^\circ C$  to  $0.6 \times 10^{-3}$  at  $1000^\circ C$  (6). The major problem in increasing Z is probably the thermal conductivity, and BP dissociates above  $1000^\circ C$ . Phosphides higher in boron have also been investigated as potential thermoelectric materials (6) and can be used at higher temperatures, so could be considered as candidates for thermoelectric power generation.

e. Sulfides: Relatively few sulfides have found commercial applications as refractory materials, but as a group they appear among the most promising for thermoelectric applications. The rare earth- and alkaline earth sulfides generally have high melting points, as do some of the refractory metals e.g. HfS. Volatilization is a serious problem and Rasneur and co-workers (7,8) report significant volatilization for  $Y_2S_3$  and  $Sc_2S_3$  respectively at temperatures above  $600^\circ C$ . However Litz and Blocher (9) report that thorium and uranium sulfides have a vapor pressure below  $10^{-7}$  atm at 2000K and that CeS,  $Ce_3S_4$ ,  $Hf_2S_3$ ,  $Zr_2S_3$  and BaS have vapor pressures below  $10^{-7}$  atom at 1500K. However, their latter list also includes Nb, Y, and Sc sulfides so should be treated with caution. A further problem with many sulfides which leads to lack of reproducibility of the data is that they tend to oxidize very readily. However cerium, thorium and uranium sulfide crucibles have been fabricated, apparently for the Manhattan project (9) and are stable in vacuum to  $1900^\circ C$ . Plots of the melting points and vapor pressures of selected sulfides are shown in Fig. 1. The data (10) are for the compound expected to have the most stable cation valence. Ba, Ce and Nd sulfides have the lowest volatility of those listed, although the vapor pressure ( $10^{-3}$  mm Hg at

ORIGIN OF POOR...

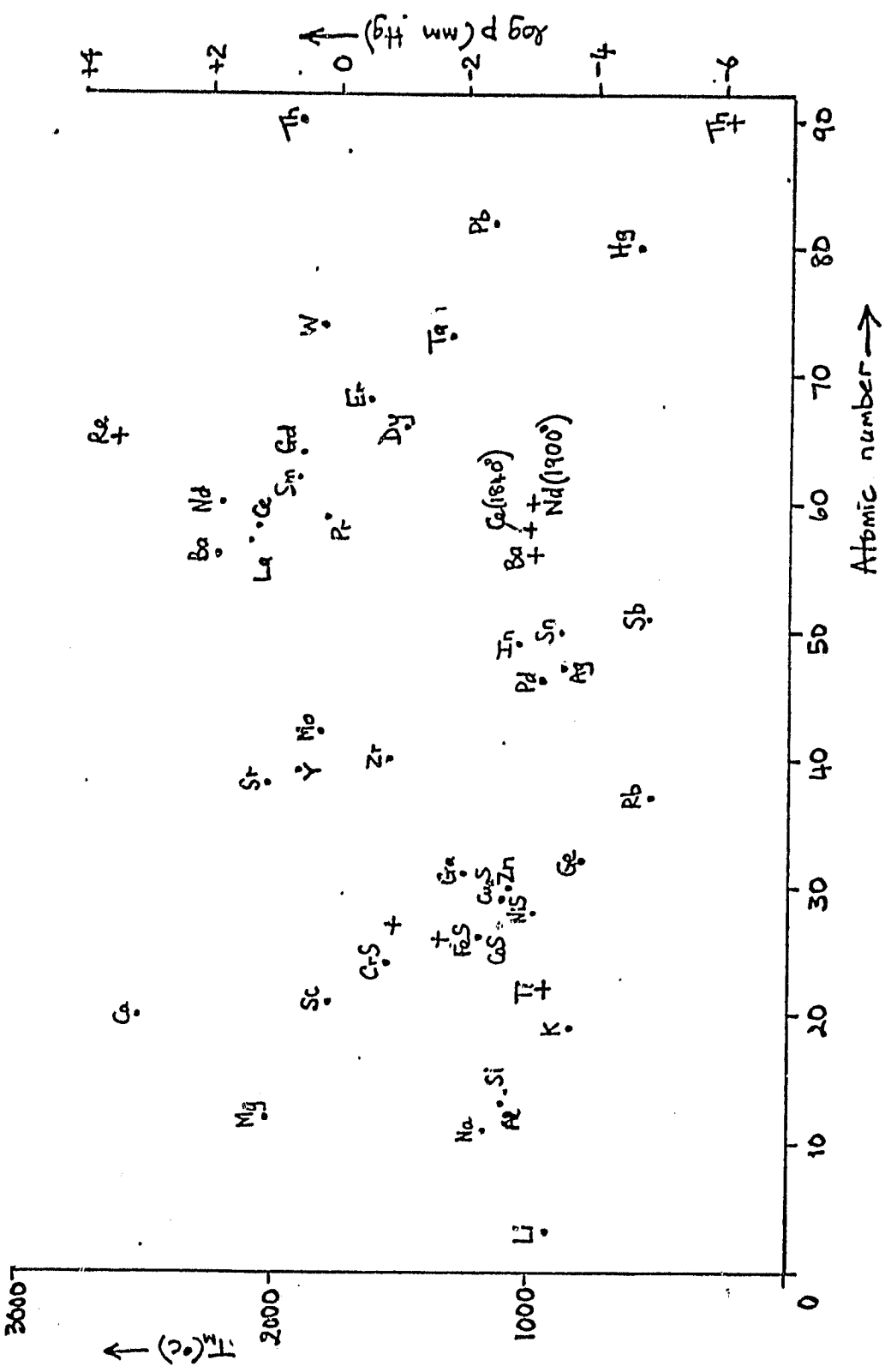


Fig. 1. Melting point  $T_m$  (°) and vapor pressure p (+) for refractory sulfides.

1600°C, 1840°C and 1900°C respectively) may be too high for very long term operation.  $\text{Th}_2\text{S}_3$  has a particularly low vapor pressure of  $10^{-6}$  mm Hg at 1600°C. Fig. 2 shows electrical and thermal conductivity data for refractory sulfides. The electrical conductivity varies from metallic conductors (CrS, FeS) to insulators (e.g.  $\text{Nd}_2\text{S}_3$ ,  $\text{Sm}_2\text{S}_3$ ). The thermal conductivity is generally in the range 10-100 mW  $\text{cm}^{-2}$  at room temperature. The optical absorption edge was recently measured (11) for a series of binary rare earth sulfides and of ternary sulfides ( $R$  = rare earth)  $\text{M}^{2+}\text{R}_2\text{S}_4$  with  $M$  = Sr, Mg and Cd. The optical bandgap of the binary materials varies from about 1.7 eV for  $\text{Nd}_2\text{S}_3$  and  $\text{Pr}_2\text{S}_3$  to 3.18 eV for  $\text{Lu}_2\text{S}_3$ . Bandgaps of the ternary materials are normally higher, the  $\text{SrR}_2\text{S}_4$  compounds with  $\text{Th}_3\text{P}_4$  structure having bandgaps from 2.14 eV ( $\text{SrCe}_2\text{S}_4$ ) to 2.82 eV ( $\text{SrLa}_2\text{S}_4$ ).

The greatest interest for thermoelectric applications has been shown in the rare earth chalcogenides, with formula between  $\text{R}_2\text{S}_3$  and  $\text{R}_3\text{S}_4$ . These materials have been reviewed by several authors, for example Flahaut (11) and Golubkov (12). The materials which appear particularly appropriate for high-temperature thermoelectric applications are those which have the  $\text{Th}_3\text{P}_4$  (cubic)  $\gamma$  - phase, with  $4\text{R}_{2.67}\text{S}_4$  formula units in each unit cell. This structure may persist throughout the  $\text{R}_2\text{S}_3$  to  $\text{R}_3\text{S}_4$  composition range, with increasing divalent ion concentration and decreasing vacancy concentration as  $x$  decreases in the general formula  $\text{R}_{3-x}\text{S}_4$ . The  $\gamma$  phase may be exhibited by the light rare earths from La ( $Z = 57$ ) to Dy ( $Z = 66$ ). Phase transformations in the temperature range of interest are a limiting factor and the  $\gamma$ -phase may be metastable. Traces of oxygen and divalent cations can influence the phase diagram.

The  $\text{R}_2\text{S}_3$  compositions are electrical insulators, but highly conducting materials can be obtained with compositions closer to  $\text{R}_3\text{S}_4$ . These latter materials show a decrease in electrical conductivity with increase in temperature. The Seebeck coefficient, which is normally n-type, increases linearly with temperature and can reach values of around 100  $\mu\text{V}/\text{deg}$  at 1000K (12). The Seebeck coefficient can be explained by the formula for metallic conductors

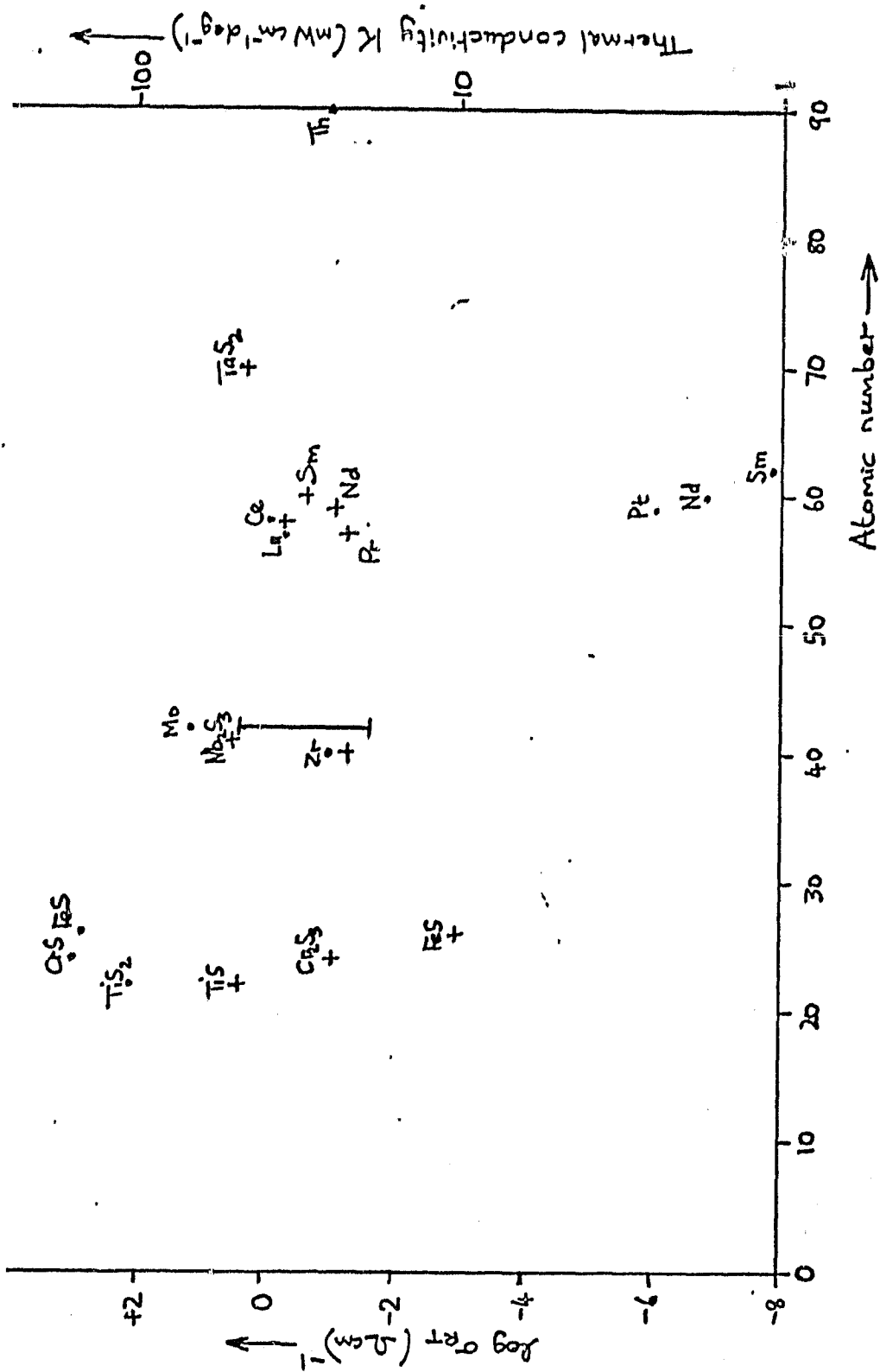


Fig. 2. Room temperature electrical conductivity  $\sigma_{RT}$  (•) and thermal conductivity  $K$  (+) for refractory sulfides.

Table 1: Electrical Properties of Rare Earth Chalcogenides (12)

Compound	Conductivity $\sigma$ (ohm cm) <sup>-1</sup>	Seebeck Coeff $-\alpha$ ( $\mu$ V/deg)	Carrier Conc		Mobility $\mu$ (cm <sup>2</sup> V <sup>-1</sup> s <sup>-1</sup> )	Effective Mass $m^*/m$
			n x 10 <sup>-21</sup>	Expt. Calc.		
La <sub>3</sub> S <sub>4</sub>	2300	35	4.0	6.0	3.5	2.6
Ce <sub>3</sub> S <sub>4</sub>	3000	20	5.0	6.2	3.3	2.8
Pr <sub>3</sub> S <sub>4</sub>	1650	20	-	6.3	-	-
Nd <sub>3</sub> S <sub>4</sub>	2300	22	4.5	6.5	3.2	2.7
La <sub>3</sub> Se <sub>4</sub>	2000	-	5.4	-	-	1.3
Ce <sub>3</sub> Se <sub>4</sub>	2620	20	-	-	-	-
Pr <sub>3</sub> Se <sub>4</sub>	2100	23	5.0	5.6	2.6	2.6
La <sub>3</sub> Te <sub>4</sub>	2940	30	1.7	4.5	11.5	1.8
Ce <sub>3</sub> Te <sub>4</sub>	10900	26	2.8	4.6	4.2	2.1
Pr <sub>3</sub> Te <sub>4</sub>	1700	26	1.7	4.7	6.2	1.6
Nd <sub>3</sub> Te <sub>4</sub>	{2200 3900}	23 5	2.8 6.0	4.8	5.0 4.1	2.0
Gd <sub>3</sub> Te <sub>4</sub>	1200	20	1.0	-	7.1	-
Dy <sub>3</sub> Te <sub>4</sub>	965	8	-	-	-	-

$$\alpha = \frac{8\pi^2}{3eh^2} m^* \left(\frac{\pi}{3n}\right)^{2/3} \quad (3)$$

where  $m^*$  is the effective mass. Values of  $m^*/m$  together with  $\sigma$ ,  $\alpha$  and the mobility  $\mu$  at 300K are listed in Table 1 for a range of chalcogenides of formula  $R_3X_4$ . The general conclusion appears to be that a metallic (= highly degenerate semiconductor) expression adequately explains electrical conduction in the  $R_3X_4$  materials.

The thermal conductivity of the rare earth chalcogenides is very low, and tends to decrease with increasing atomic weight as shown in the data of Fig. 3. This suggests that selenides and tellurides are preferable to sulfides, although their melting points are generally lower. In all cases the figure of merit  $\bar{Z}$  (=ZT) tends to change rapidly with temperature and reaches reasonable values ( $Z < 1$ ) only at the high-temperature end of the operating range 700 - 1500K. Two examples are shown in Fig. 4 (12, 13). The decrease in  $\bar{Z}$  at the lower temperatures arises from the small values of Seebeck coefficient  $\alpha$ , since  $\sigma$  in fact decreases with T. If  $\sigma \propto n$  and  $\alpha \propto n^{-2/3}$ , the optimum value of  $\alpha^2\sigma$  should occur at some low value of  $n$ . In fact Eq. (3) becomes invalid as  $n$  is decreased, and  $\mu$  will depend on  $n$ , so there will exist an optimum value of  $n$  for some composition between  $R_2X_3$  and  $R_3X_4$ .

f. Borides: Boron compounds generally appear to be the most promising for high temperature thermoelectric applications, on account of their high melting points (usually in the range 1900 - 3000°C) and low volatility. Low-boron compositions, for example those of general formula  $MB$  or  $MB_2$ , are metallic conductors. The  $MB_6$  compounds, notably the rare earth hexaborides, are also highly conducting compounds in which the boron atoms form octahedral groups enclosing the rare earth atoms. The electrical properties of the hexaborides can be broadly understood from the molecular orbital calculations of Longuet-Higgins and Roberts (14). The boron valence band formed from the six boron atoms per unit cell requires a total of 20 electrons (6 electrons to form shorter covalent bonds with adjacent octahedra and 14 electrons to fill the 7 bonding molecular orbitals of the octahedral group). Two additional electrons per cation are therefore

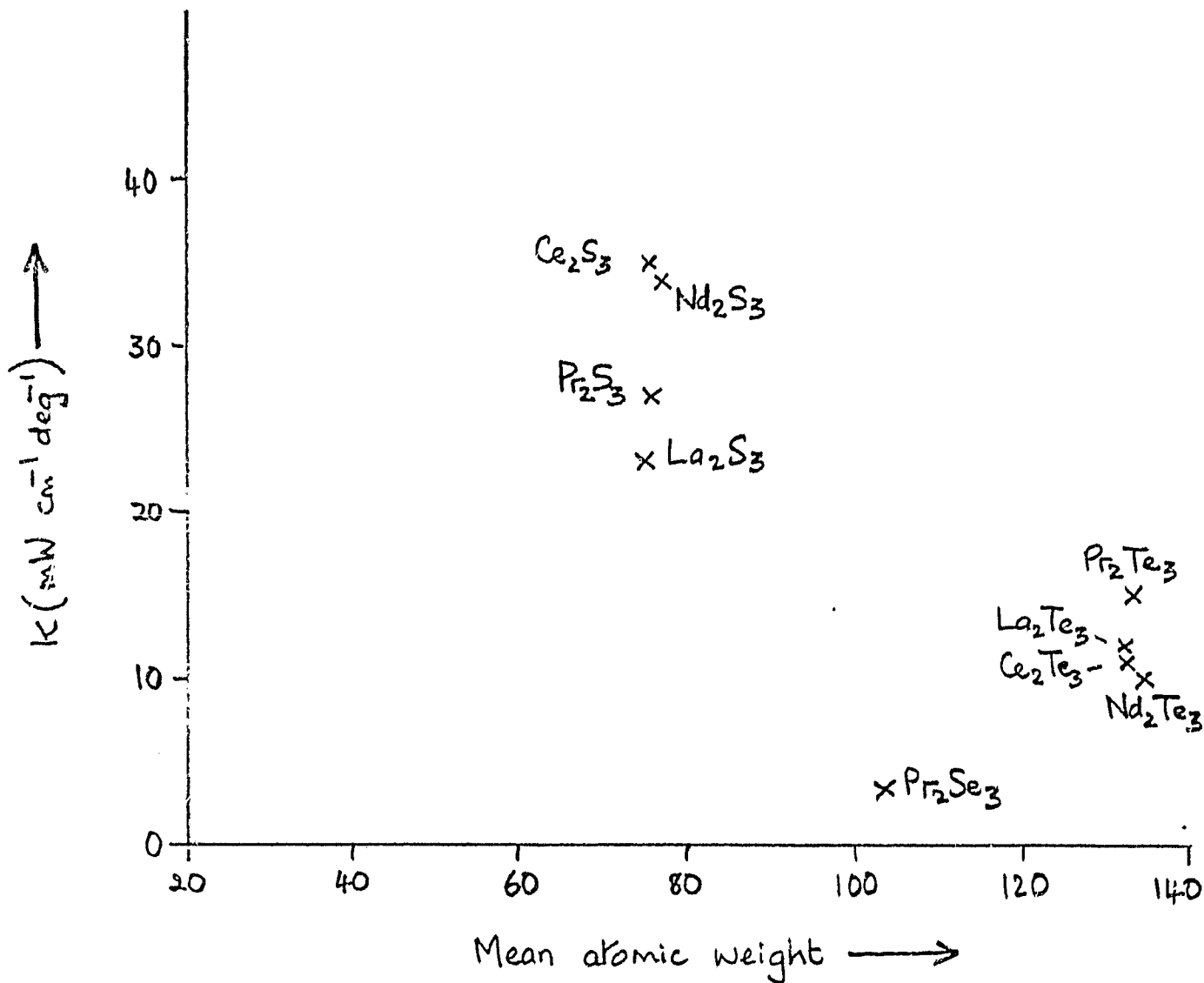


Fig. 3. Thermal conductivity K of some rare earth chalcogenides as a function of mean atomic weight.

CRITERIA  
OF PERFORMANCE

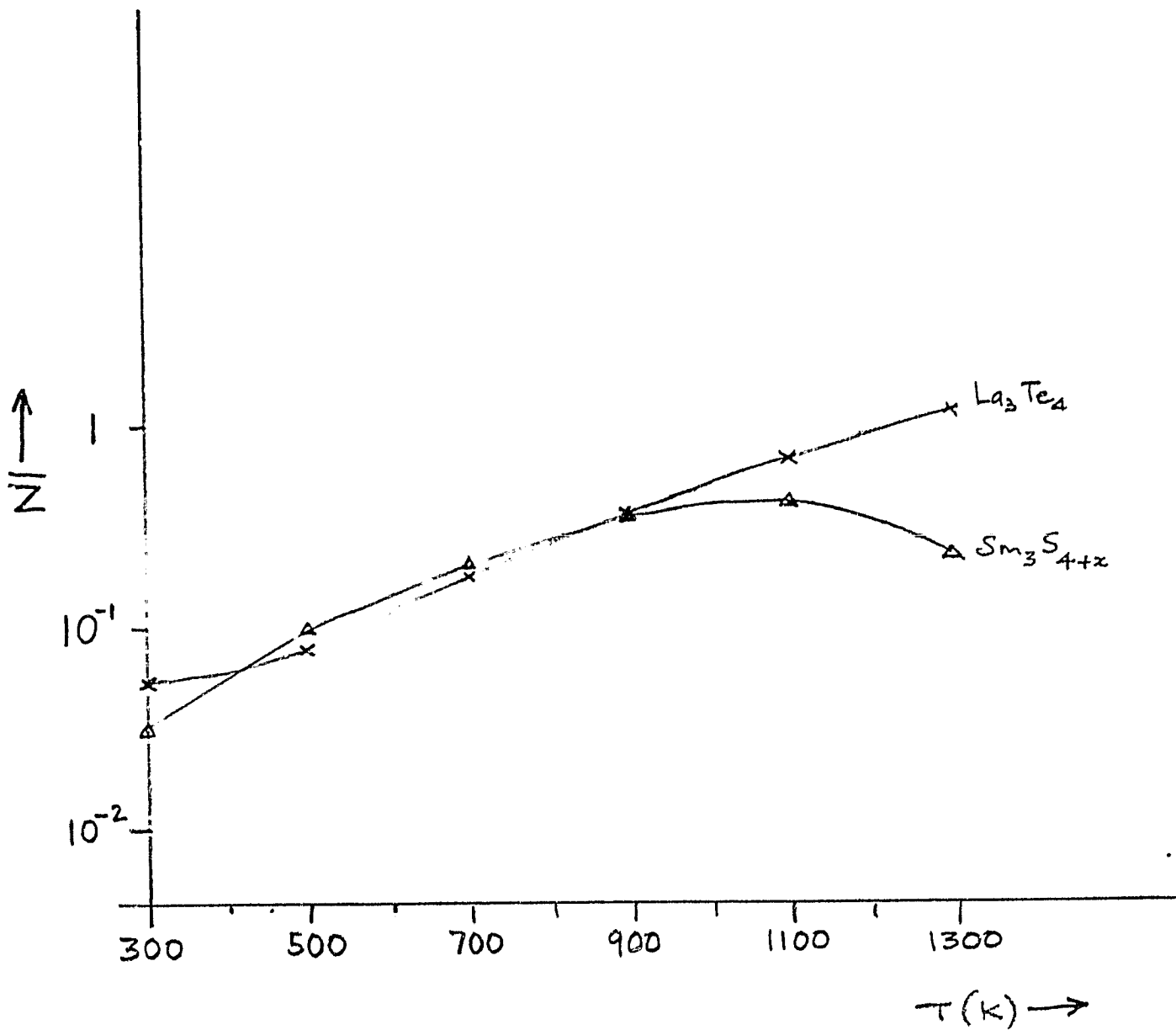


Fig. 4. Figure of merit  $\bar{Z}$  ( $=ZT$ ) versus temperature for  $\text{La}_3\text{Te}_4$  and  $\text{Sm}_3\text{S}_4$ .

required to fill the bonding orbitals and so stabilize the structure. The antibonding conduction band is expected to be well above the valence band. According to this model, the rare earth hexaborides ( $\text{LaB}_6$ ,  $\text{SmB}_6$  etc.) are normally metallic conductors since the trivalent rare earth ion contributes one conduction electron per formula unit. The alkaline earth hexaborides are expected to be semiconductors and this is found experimentally. Table 2 shows some data on hexaborides from Samsonov (15). This confirms that the rare earth hexaborides have low Seebeck coefficients as expected for metallic conductors, but the alkaline earth hexaborides, especially  $\text{SrB}_6$  and  $\text{BaB}_6$ , are of interest because of the high carrier mobility. It should be commented also that the Hall and Seebeck data both indicate n-type conduction, which is unusual for borides. Johnson and Daane (16) reported rather higher values of resistivity than those in the Russian work. At 1000 K,  $\rho$  was around  $10^2$  ohm cm for  $\text{SrB}_6$  and 300 ohm cm for  $\text{CaB}_6$ . The activation energy for conduction was 0.40 eV for  $\text{CaB}_6$ , 0.38 eV for  $\text{SrB}_6$  and 0.12 eV for  $\text{BaB}_6$ , these values being rather low for an ideal high temperature thermoelectric. The unit cell is cubic with lattice constant of around 4.2 Å, so the thermal conductivity is also expected to be low.

Dodecaborides, such as  $\text{UB}_{12}$ , and phases richer in boron than hexaborides tend to have structures in which the boron atoms occur fully or partially in dodecahedral  $\text{B}_{12}$  "superatoms". Most  $\text{MB}_{12}$  compounds are semiconductors e.g.  $\text{AlB}_{12}$  and have been considered as candidates for high temperature thermoelectric applications. Rare earth metals usually form, in addition to  $\text{RB}_{12}$  compounds, the complex cubic  $\text{YB}_{68}$  structure with  $1628 \pm 4$  boron atoms per unit cell (17). This structure appears to have the lowest thermal conductivity of any boron phase but has rather low electrical conductivity. Doping to a level of  $10^{19} - 10^{20} \text{ cm}^{-3}$  to achieve a higher electrical conductivity appears impossible without destroying the crystal structure. Rare earth borides have been recently reviewed by Spear (18).

In general, it seems that the most likely borides to meet the requirements for high temperature thermoelectric generation have compositions between  $\text{MB}_6$  (possibly  $\text{MB}_4$ ) and heavily-doped boron. We

Table 2: Electrical Properties of Hexaborides  
at Room Temperature (15)

<u>Metal</u>	<u>Resistivity</u> ( $\mu\text{ohm cm}$ )	<u>Hall Coeff</u> ( $\times 10^4 \text{cc/coul}$ )	<u>Seebeck Coeff</u> ( $\mu\text{V/deg}$ )	<u>Carrier Mobility</u> ( $\text{cm}^2\text{V}^{-1}\text{s}^{-1}$ )
Ca	222	-91.0	-32.8	41.0
Sr	111	-76.3	-30.3	68.7
Ba	77	-57.5	-26.2	74.7
Y	40	- 4.6	- 0.5	11.4
La	15	- 5.0	+ 0.1	33.1
Ce	29	- 4.2	+ 0.3	14.2
Pr	20	- 4.3	- 0.6	22.2
Nd	20	- 4.3	+ 0.4	22.0
Sm	207	+ 1.5	+ 7.6	0.74
Eu	85	-50.2	-17.7	59.3
Gd	45	- 4.4	$\pm$ 0.1	9.8
Tb	37	- 4.6	- 1.1	12.2
Yb	47	-83.6	-25.5	179.4

treat the problem of finding an appropriate dopant for  $\beta$ -boron in a separate subsection.

### 3. Electronic Structure of Boron

A theory of phenomena involving electronic transport in a compound generally proceeds from a theory of its static electronic structure. Recently, Harrison [19, 20] has developed a simple, but quantitative, tight-binding theory of electronic structure of solids, that applies generally when s- and p- orbitals dominate the bonding. At the heart of the theory are universal matrix elements, which depend only on the internuclear distance. Repulsion comes from nonorthogonality of the basic states, and is calculated from Extended Hückel Theory. This theory was applied to an icosahedron of boron, which forms in many of its compounds, and so seems likely to be central to the electronic structure of the whole solid. It would be a difficult extension of this theory to treat  $\alpha$ - and  $\beta$ -boron, particularly the latter in view of its complex structure.

The electronic structure of the icosahedron may be largely understood as consisting of 12 radially directed sp hybrids at each lattice site, which link the icosahedron with whatever is external to it, and form the valence band through a smaller mutual coupling. These hybrids are only weakly coupled to the remaining 36 orbitals largely internal to the icosahedron. Of the internal orbitals, 13 are bonding and 23 are antibonding. This much Longuet-Higgins and Roberts (21) found in an earlier calculation, but they did not have a quantitative theory for the matrix elements and nonorthogonality. Because the matrix elements for all of the internal bonding states are large in comparison the external hybrid matrix elements, Longuet-Higgins reasonably concluded the internal states lie well below the valence band and behave something like core states. Consequently they predicted that the icosahedron has a net charge of -2, since the 12 atoms of the icosahedron have available only 24 electrons to the internal orbitals.

However, the internal orbitals contain a single internal molecular orbital of spherical ( $A_g$ ) symmetry, and which turns out to

have an unusually large nonorthogonality. This greatly weakens its coupling strength to something comparable to the coupling of the external hybrids. The 12 external hybrids also contain a single molecular orbital that transforms according to  $A_g$  symmetry, and this couples to the internal state with a coupling of approximately 1 eV. These levels are thus split into a bond-antibond pair, probably the deeper one forming part of the valence band and the other a very narrow, empty band just above the valence band edge.

This explains how the icosahedron is not charged doubly negative, as Longuet-Higgins concluded. Indeed, he predicted from this that a lattice composed strictly of icosahedra would not form, although in fact the  $\alpha$ -boron structure is close to a cubic close packed array of boron icosahedra, with no interstitial atoms.

These unoccupied levels are probably intimately involved in the electronic transport. It is possible that an electron is mostly localized in one of these states, and hops from one icosahedron to an adjacent one. So far, some gaps in Harrison's theory have precluded us from accurately resolving the relative positions of these critical energy levels. Some new tools are now being developed which should permit us to satisfactorily address this problem.

One important feature in our method of solution was to make use only of a five-fold rotational symmetry of the icosahedron (which forms a cyclic group), and the inversion, rather than exploiting the full symmetry with 10 irreducible representations and 120 operations. Since this solution does not rely on the full symmetry of the icosahedron, it is readily adapted to the calculation of properties which retain the five-fold rotational symmetry, even if they destroy the full symmetry. We have included a carbon atom as a substitutional impurity and found that it requires a large energy of formation, making it an unlikely candidate as a location for a substitutional dopant. Also force constants that involve squashing or twisting the icosahedron may be calculated from fairly direct extensions of the first solution.

#### 4. A Conceptual Base for Enhanced Phonon Scattering

To optimize the thermoelectric figure-of-merit of a material it is necessary to reduce the thermal conductivity, while increasing the electrical conductivity and maintaining the Seebeck coefficient at a satisfactory level. Since charge carriers contribute to both thermal and electrical conductivity, the charge carrier contribution to the thermal conductivity can only be reduced to some lowest value consistent with maintaining adequate electrical conductivity. It is therefore important that the lattice contribution to the thermal conductivity should be reduced to a small amount relative to the residual charge carrier contribution. If this situation can be achieved, the final properties of the optimized material are almost, if not completely, determined by the behavior of the charge carriers.

According to Slack et al (21), lattice thermal conductivity is dominated by acoustic phonons. This means that materials with complex unit cells, which have a large number of optical phonons relative to the three types of acoustic phonons, are to be favored. Lattice thermal conductivity is determined by the mean free path of the acoustic phonons, established by interphonon scattering. This is a complex phenomenon even in the simpler materials, such as the cubic doped SiGe alloys (21, 22). For complex structures such as the boron compounds, the most that can be expected theoretically is the establishment of a conceptual base (or a set of guidelines) to be used in choosing the types of defects to be tried experimentally in an effort to enhance the interphonon scattering.

An excellent review of thermal conductivity in solids has been written by Berman (23), in which Chapter 8 (The Thermal Conductivity of Imperfect Crystals) is particularly relevant to the present purpose. Lattice thermal conductivity is analyzed in terms of phonon relaxation times (which can be expressed in terms of mean free paths) due to various scattering mechanisms. Relaxation times refer to the return to thermal equilibrium of a perturbed phonon distribution, based on the assumption that the scattering process restores the distribution to equilibrium at a rate proportional to the departure

from equilibrium. In a defect-free crystal, scattering is due to lattice nonlinearity and care must be taken to distinguish Umklapp processes and normal processes. Only the first of these tends to return the phonon distribution to equilibrium, but normal processes still exert a subtle influence in the presence of equilibrating scattering processes.

Analysis of lattice thermal conductivity in imperfect crystals begins with a study of scattering from the various types of defects and proceeds by incorporating the scattering cross-sections into expressions for relaxation time that can be used in evaluating the conductivity. Because of the enormous difficulties encountered in actual computation of thermal conductivities the analysis is reduced to its simplest terms and does not, for example, include crystal anisotropy and phonon polarization. Berman gives simple relaxation time formulas for point mass defects, point polarizability defects and anharmonic effects due to local lattice distortion.

These standard analyses are not of great utility in dealing with complicated structures such as the boron compounds, in which point defects can occupy a wide variety of substitutional sites, having coordination numbers 6, 8 and 9. Added to this are the various interstitial positions. In order to establish at least qualitative guidelines for optimum choices of defect sites it is necessary to develop some concepts regarding the effect of the defect site on phonon scattering - for both mass and stiffness defects. The starting point has been taken from the theory of elastic wave scattering from defects in continuous media (24, 25). According to this theory, the amplitude scattering coefficient for an incident elastic plane wave at frequency  $\omega$  is

$$\Gamma_{12} \sim i\omega \int_{\text{Scatterer}} (\Delta\rho v_2' \cdot v_1 + \epsilon_2' : \Delta c : \epsilon_1) dV \quad (4)$$

where  $v_1$  is the elastic displacement velocity field in the absence of the scatterer produced by an incoming plane wave along the direction of the actual scattered plane and  $v_2'$  is the elastic field in the presence of the scatterer due to the actual incident plane wave.

Corresponding elastic strains are  $\epsilon_1$  and  $\epsilon_2'$ . In the integrand,  $\Delta\rho$  is the mass density defect of the scatterer and  $\Delta c$  is the elastic stiffness tensor defect. This result derives from the elastodynamic reciprocity relation. Such relations exist for all reciprocal linear systems, including the dynamic equations for crystal lattices in the simple physical model of Brillouin (26).

For the simple lattice model scattering formulas similar to Eq. (4) have been derived, but results in such detail could not be used at the present time for lack of knowledge of the relative spring constants in the boron compounds of interest. However, general qualitative conclusions can be drawn immediately from Eq. (4) and conjectures can be made by imagining its analogous form for the lattice case. In the derivative of Eq. (4), resonance of the scatterer was not excluded and it is clearly seen that resonance build-up of the primed fields greatly increases the scattering. Furthermore, the fact that polarizations are explicitly included shows that selection rules for interpolarization coupling are contained in the formulation. More useful for qualitative judgements as to the choice of optimum defect sites are observations that a density defect  $\Delta\rho$  produces maximum scattering at a point of maximum displacement velocity and an elastic stiffness tensor defect produces maximum scattering at a point of maximum strain. For the lattice problem these statements relate to the optimum locations of mass defects and bonding spring constant defects. As a simple example, consider the one-dimensional diatomic lattice treated by Brillouin (26). It is found that on the acoustic branch the heavier atoms move more than the lighter atoms, with the difference increasing as the zone boundary is approached. At the zone boundary itself the lighter atoms are immobile. In this case greater scattering is achieved by placing a given mass defect at the site of a heavy atom than at the site of a light atom.

The above remarks can be applied to boron compounds, where two types of atoms exist. For boron itself, where only one type of atom exists, the choice must be based on differences in spring constants within the unit cell. The example of Brillouin could be extended by

considering a one-dimensional monatomic lattice with two spring constants and then seeking criteria for optimum location of mass and spring constant defects. To apply this approach to boron and boron compounds it will be necessary to draw some conclusions regarding the relative spring constants at various sites and to attempt to deduce, qualitatively, the internal motions of the unit cell toward the upper parts of the acoustic phonon spectra. Some recent work by M. van Shilfgaard, summarized in the previous section, is a very promising start in this direction.

## B. EXTRAPOLATION FROM KNOWN MATERIALS

### 1. Lanthanum Sulfide

Our own effort to date has been concentrated on boron compounds, but it appears that  $\text{La}_{3+x}\text{S}_4$  is the most promising of the rare earth chalcogenides. The corresponding telluride  $\text{La}_{3\pm x}\text{Te}_4$  has the advantages of a lower thermal conductivity and higher carrier mobility, and Te appears the most promising element for the formation of solid solutions. The disadvantages of  $\text{La}_{3+(S, Te)}_4$  solid solutions are that the melting point is lower, and the vapor pressure may be higher. It should also be commented that the latest Soviet phase diagram (Elyseev et al) does not show  $\text{La}_2\text{Te}_3$  and so the solubility of tellurium in the  $\text{Th}_3\text{P}_4$  phase may be very limited.

Divalent ion substitution for La is also of interest since it is expected to lead to a reduction in the thermal conductivity. The ionic radius of  $\text{La}^{3+}$  is 1.04 Å which is comparable with that of  $\text{Ca}^{2+}$  (0.94 Å) or  $\text{Sr}^{2+}$  (1.10 Å). The lattice constant of  $\text{CaLa}_2\text{S}_4$  is in fact closest to that of  $\text{La}_3\text{S}_4$ . It could also be expected that  $\text{Ba}^{2+}$ , with a slightly higher ionic radius (1.26 Å) will substitute to some extent for lanthanum and this is expected to have the greatest influence on the thermal conductivity.

The synthesis of complex sulfides of general formula  $\text{RBC}_3\text{S}_7$  has also been reported (11). These have a tetragonal unit cell and are prepared by quenching the melts and heating the resulting glasses slightly above the crystallization temperature. This fabrication

technique should yield pore-free materials which might be particularly appropriate for high temperature thermoelectric generation. Hexagonal compounds of general formula  $R_6B_2C_2S_{14}$  have also been prepared.

## 2. Boron Carbide

Boron carbides of formula  $B_4C-B_{10.5}C$  have been the most intensively investigated materials for high temperature thermoelectric applications and the recent GA/JPL/Sandia collaborative study has greatly advanced our understanding of their properties. In general their electrical properties (i.e. the maximum value of  $\alpha^2\sigma$ ) compare favorably with alternative materials, although the usual problem is encountered of a decrease in  $\alpha^2\sigma$  at the lower temperatures due to the decrease in  $\mu$ . We have focussed our attention on the thermal conductivity and are seeking to establish principles on which suitable dopants for this and other candidate materials may be selected.

## 3. $\beta$ -Boron

Doped  $\beta$ -boron is a candidate high temperature thermoelectric material, and  $\beta$ -boron is the obvious model material for the study of dopant behavior in high-boron materials, since  $\alpha$ -boron is much more difficult to prepare. Silicon doped  $\beta$ -boron has been considered of particular interest in this investigation because of the high figure of merit reported for  $SiB_{14}$  (presumed to be the limiting silicon concentration in  $\beta$ -boron) by Pistoulet and co-workers (28).

What is particularly lacking is the correlation between the type of dopant, site occupancy, and the effect on electrical and thermal conduction properties. Most of the detailed studies to date have been concerned only with structural aspects, that is with the use of x-ray diffraction to determine the site occupancy.  $\beta$ -boron itself has 15 distinct atomic sites, those labelled 1-6 describing sites in the icosahedra, 7-14 in the condensed polyhedra which are unique to the  $\beta$ -boron structure, and site 15 being in the center of the rhombohedral (or hexagonal) unit cell. In addition, Hoard et al (29) report a 16th site with a 33% probability of occupation, located close to the icosahedron at the ends of the rhombohedral cell. Site 13 has only a

2/3 probability of occupation, according to this study.

The  $\beta$ -boron structure has eight vacant interstitial sites normally available for occupation, which are listed in Table 3 together with their hexagonal coordinates. (The c axis of the hexagonal cell is the long diagonal axis of the rhombohedral cell.) The interstitial sites are labelled A, D, E, F, G and the lattice sites  $B_1$ ,  $B_2$  etc. Also listed in Table 3 are the results of x-ray diffraction investigations to determine site occupancy in doped  $\beta$ -boron. The materials were normally made by melting, and small crystals were extracted from the resulting polycrystalline mass.

It can be seen that atoms normally occupy one or more (typically two) interstitial sites, especially the D sites which are the largest "holes" in  $\beta$ -boron. These are located in the mid-plane of the unit cell near to site 15. The other holes which are occupied by several different atoms are the  $A_1$  sites, located along the c-axis of the hexagonal cell between the set of 3 icosahedra adjacent to the icosahedron centered on (0,0,0), and the E sites which are also on the c-axis midway between the origin and the center of the hexagonal cell. Many dopants occupy the largest  $A_1$  and D sites, but Cu, Mn, Sc and Zr all partially occupy the E holes. Ge, Sc and Si partially occupy substitutional sites, and an additional source of disorder is the fractional occupation of the  $B_{13}$  sites, which varies from 53% in Zr-doped material to 74% in Si-doped  $\beta$ -boron. We have made a model of the  $\beta$ -boron structure to help in the understanding of doping and other structure-related effects (see Fig. 5)

Fig. 6 shows the c/a ratio (hexagonal indexing) for various dopants in  $\beta$ -boron. Data for a wide range of concentrations is available only for Cu (30) and Si (31). The behavior of these two dopants is very different, since Cu changes the a and c dimensions roughly equally while Si expands the a axis but has little effect on the length of the hexagonal cell. This rather anomalous behavior of Si appears to arise from the unexpected tendency of these atoms to occupy sites which are closely located in the cell, the substitutional  $B_1$  sites and the neighboring  $A_1$  holes. This proximity must cause local stress which is relieved by expansion along the a axis. Most

Table 3: SITE OCCUPANCY IN  $\beta$  - BORON

Number	Dopant: Composition: Ref. #:		$\beta$ -B 1	Cr CrB <sub>4</sub> 1 2	Cu CuB <sub>4</sub> 2 3	Fe FeB <sub>4</sub> 9 4	Ge GeB <sub>5</sub> 90 5	Mn MnB <sub>6</sub> 23 6	Sc ScB <sub>7</sub> 28 7	Si SiB <sub>8</sub> 36 8	Zr ZrB <sub>9</sub> 51 9	Approx. Hole. Diam. A
	Site Hex. Coordinates											
B1	.17	.17 .17	1	1		1	.97B .03Ge	1	1	.87B .13Si	1	
B4	.23	.25 .34	1	1		1	1	.94B .06Sc			1	
B13	.06	.11 -.44	.67	.72		.73	.72	.65	.61	.74	.53	
B16 (G)	.05	.11 .12	.33	-		-	-	-	-	-	.14	
A1	0	0 .14	-	.72	.08	.51	.21	.26	-	.46	-	2.54
A2	.11	.22 .10	-	-	-	-	-	-	-	.05	-	2.36
A3	.28	.25 .05	-	-	-	-	-	-	-	-	-	2.06
D	.21	.41 .17	-	.18	.21	.18	.02	.43	.31	-	.28	2.70
E	0	0 .25	-	-	.36	-	-	.66	.73	-	.18	2.14
F1	.07	.13 .25	-	-	-	-	-	-	-	-	-	2.48
F2	.12	.23 .25	-	-	-	-	-	-	-	-	-	1.82

References

1. J. L. Hoard, D. B. Sullenger, C. H. L. Kennard & R. E. Hughes, J. Sol. St. Chem., 1(1970)268.
2. S. Andersson & T. Lundstrom, J. Sol. St. Chem. 2(1970)603.
3. T. Lundstrom & L. E. Tergenius, J. Less-Comm. Met. 47(1976)23.
4. B. Callmer & T. Lundstrom, J. Sol. St. Chem. 17(1976)165.
5. T. Lundstrom & L. E. Tergenius, J. Less. Comm. Met. 82(1981)341.
6. S. Andersson & B. Callmer, J. Sol. St. Chem. 10(1974)219.
7. B. Callmer, J. Sol. St. Chem. 23(1978)391.
8. M. Vlasse & J. C. Viala, J. Sol. St. Chem. 37(1981)181.
9. B. Callmer, L. E. Tergenius & J. O. Thomas, J. Sol. St. Chem. 26(1978)275.

ORIGINAL MODEL  
OF POOR QUALITY

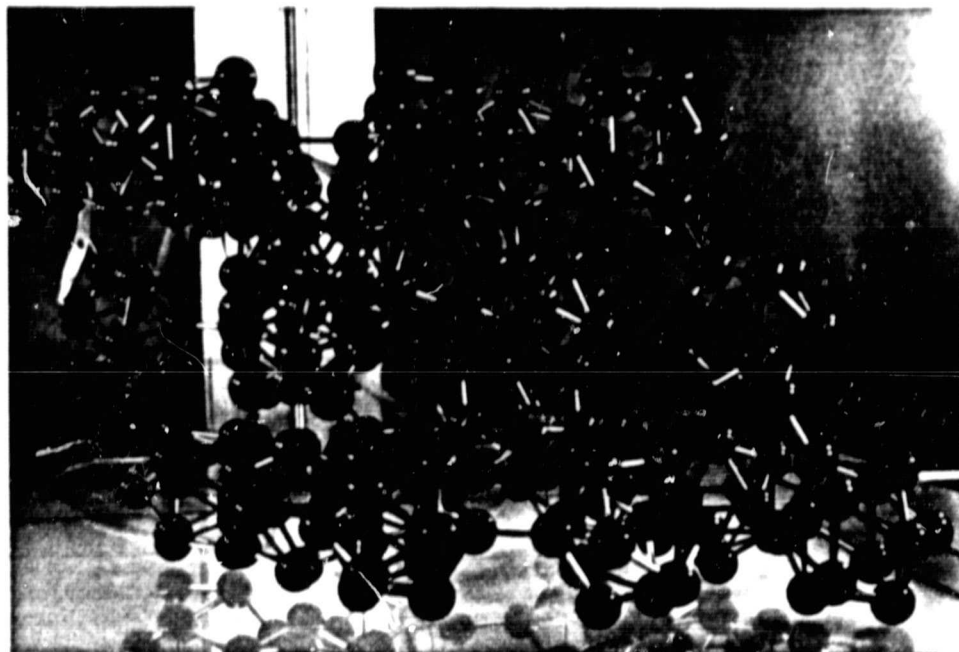


Fig. 5. Model of  $\beta$ -boron structure made by A. P. Ariotedjo in our laboratory.

ORIGINAL SOURCE  
OF PDB: 67-1000

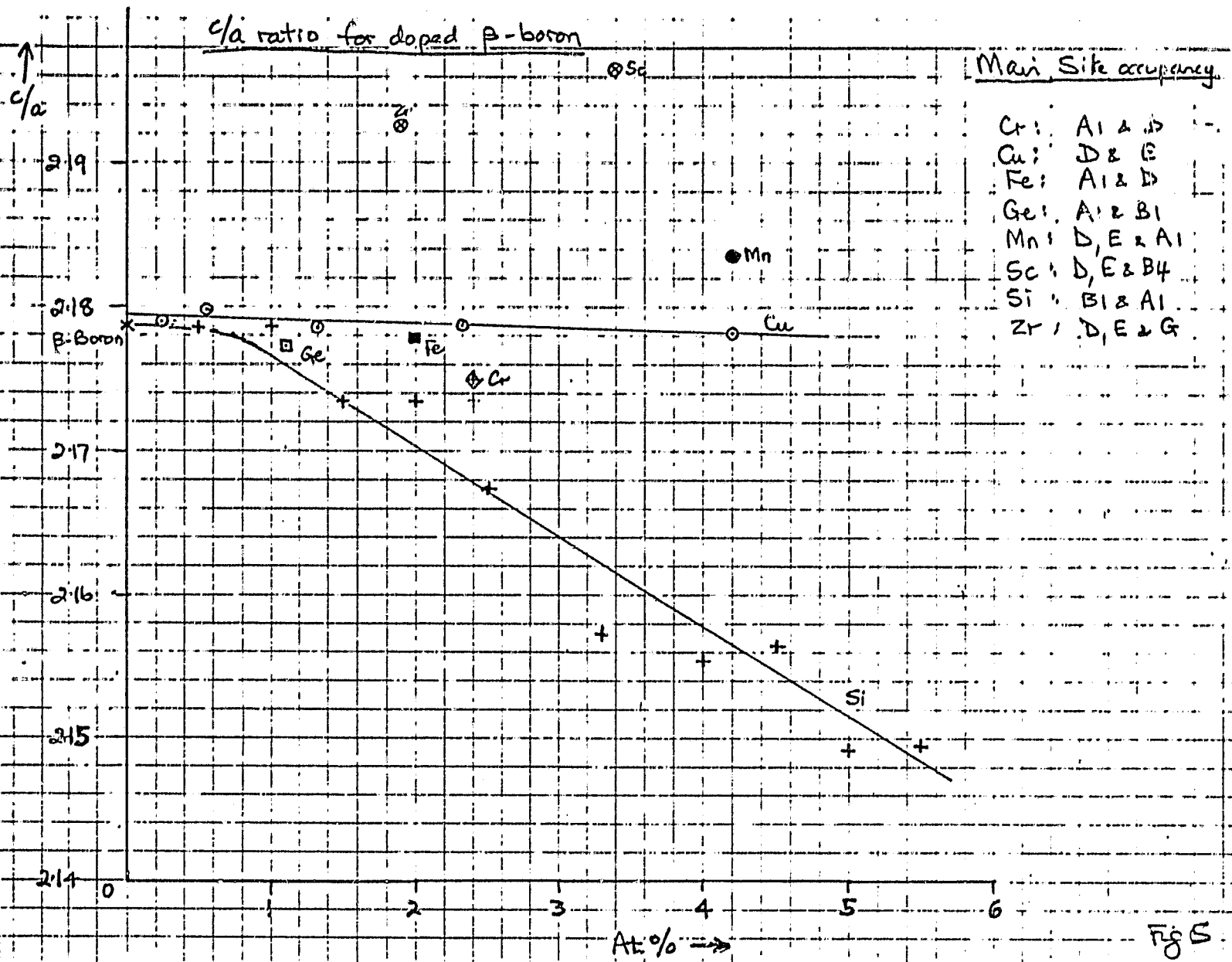


Fig. 6. Ratio  $c/a$  for various dopants in  $\beta$ -boron. Lines plotted are for Cu- ( $\theta$ ) and Si (+) doping. The table summarizes the most important sites for the various dopants.

atoms behave like Cu in having a similar effect on a and c dimensions, but Sc and Zr act oppositely to Si i.e. elongate the c axis. This effect may be associated with a particularly large occupation of the D holes.

Also of interest is the effect of the various dopants on the atomic volume (Fig. 7). All dopants cause an increase in this parameter compared with that of undoped  $\beta$ -boron, but the data fall into two groups - a relatively large slope equal to 0.066% per % dopant and a smaller change of .035% per % dopant. The former slope is that of the Si data, the latter that of the Cu. Since covalent radii tend to be much larger than ionic, we may tentatively conclude that the former group (Si, Ge, Zr) are covalently bonded in boron while the latter group (Cu, Cr, Fe, Mn) are ionized. Scandium occupies an intermediate position.

It may be expected from this conclusion that the transition metals cause a large change in the electrical conductivity of  $\beta$ -boron and this is confirmed by the GE data (32). Addition of 1% of the transition metals Co, Fe and especially Cr and V was found to cause a large increase in the room temperature conductivity of  $\beta$ -boron whereas the increase caused by Zr and Si is lower by several orders of magnitude. The transition metal doped  $\beta$ -boron is n-type, as expected if these metals give up conduction electrons to the lattice, and the doped materials would be of practical interest except that the mobility of conduction electrons appears to drop to very low values (in comparison with holes) at temperatures above 200-300°C.

The problem of finding a good dopant which will give a high figure of merit for p-type  $\beta$ -boron still remains, and there does not yet appear to be enough data to allow generalizations on doping behavior to be firmly established. The alternative of predicting the effect of a particular dopant from first principles is a formidable task.

### C. DEVELOPMENT OF NEW CRITERIA FOR MATERIALS SELECTION

The figure of merit ( $Z$  or  $\bar{Z}$ ) is the parameter which has been traditionally used in the selection of thermoelectric generator

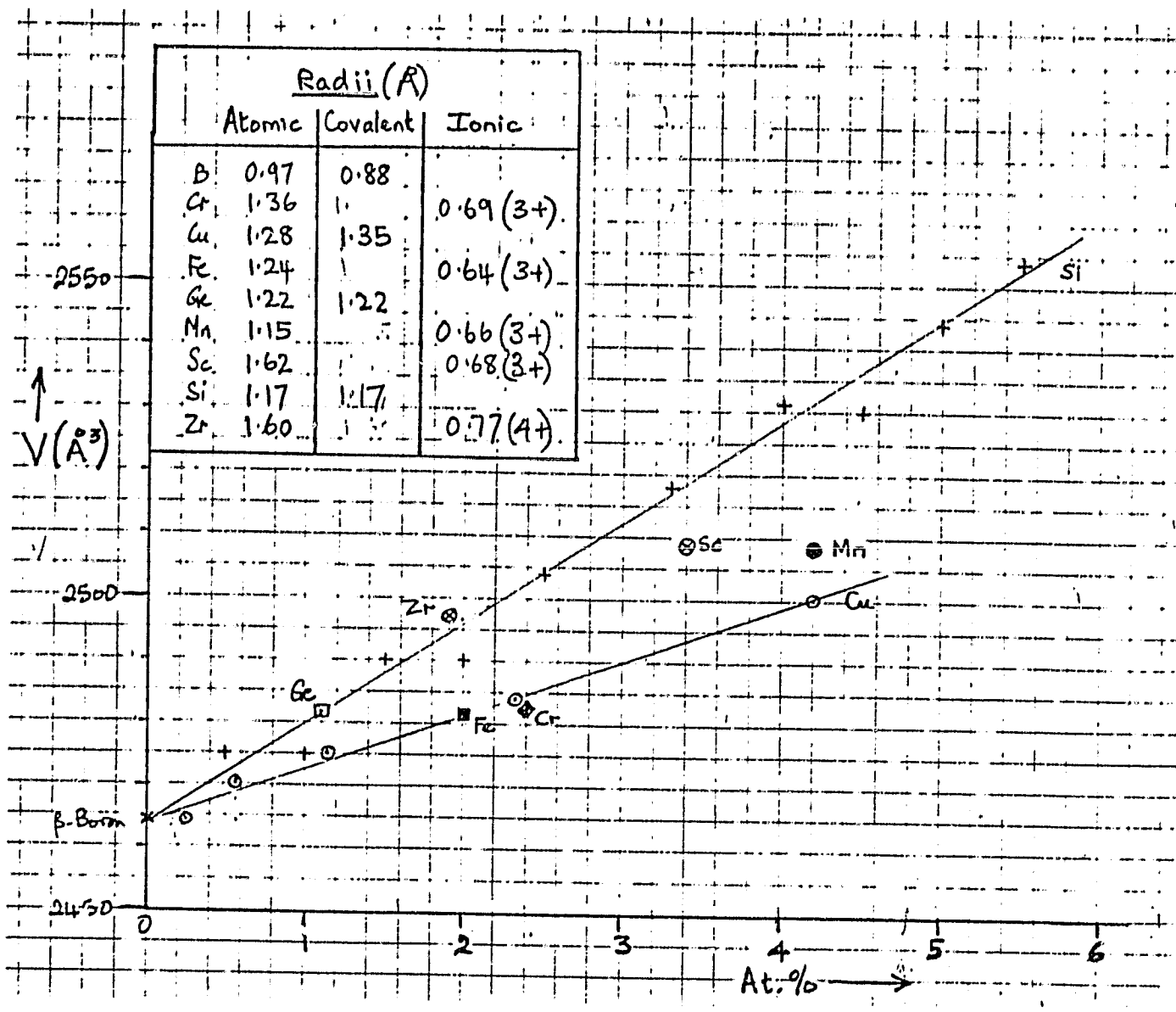


Fig. 7. Volume of the hexagonal unit cell for  $\beta$ -boron.

materials. This parameter is clearly of great help in selecting materials but we felt that it was desirable to seek alternative criteria that would be of value in materials selection. A re-evaluation of the figure of merit has been attempted by other investigators, for example by Goff and Lowney (33). They wrote the figure of merit as

$$\bar{Z} = [p(e^2TK_p/M + 1)^{-1}]^{-1} \quad (5a)$$

where  $p = M_0M_2/M_1^2$  and the M's are integrals of the form

$$M_n = -\int \sigma(E)E^n(\partial f/\partial E)dE \quad (5b)$$

Here  $f$  is the Fermi-Dirac function and  $\sigma$  the electrical conductivity over a range of energy covered by the derivative  $(\partial f/\partial E)$ . This range is about  $10kT$ .  $K_p$  in Eq. (5a) is the sum of lattice and radiation contributions to the thermal conductivity. Use of Eq. (5) requires data on the band structure and carrier scattering mechanism, and it is limited to materials which can be described as broad-band conductors.

The earlier analysis of Chasmar and Stratton (28) is, in our view, the most useful to date. It gives

$$\bar{Z} = (\eta - A)^2/[\Delta + (1/\beta E)] \quad (6a)$$

with

$$\beta = (k/e)^2T\sigma_0/\lambda_L \quad (6b)$$

Here  $\eta$  is the Fermi energy in units of  $kT$ ,  $\Delta$  an integral which determines the electronic contribution to the thermal conductivity and  $\sigma_0$  the electrical conductivity extrapolated to infinite temperature. The 'material factor'  $\beta$  can be written as

$$\beta = Ne (k/e)^2T\mu_c/\lambda_L \quad (7)$$

with  $N$  the density of states,  $\mu_c$  the carrier mobility and  $\lambda_L$  the lattice contribution to the thermal conductivity. This equation therefore suggests that a good thermoelectric material will have a high carrier mobility, low lattice thermal conductivity and a high density of states. Although Eq. (7) was derived for a broad band semiconductor, it may be anticipated that the above conclusion will

hold more generally. However the assumption that  $N \propto m^*3/2$ , with  $m^*$  the effective mass of the carriers, will not hold for a small polaron conductor. Golikova et al (35) use an equation

$$Z = \frac{k^2}{e} \frac{4}{\exp(2)} N \frac{\mu}{\lambda_L} \quad (8)$$

in the case of hopping conduction. (Eq. (8) also stresses the importance of  $N\mu/\lambda_L$ , but these authors do not quote the origin of their formulas).

Fig. 8 gives an impression of the parameters required of a material which will give an adequate thermoelectric conversion efficiency.  $\bar{Z}$  is calculated for one temperature (1000K) and assuming that  $kA/e$  (Eq. 2) has a value of 40  $\mu\text{V}/\text{deg}$ . It is also assumed that  $N = 10^{22} \text{ cm}^{-3}$ . The graph shows the changes in  $\bar{Z}$  when  $\mu = 0.1, 1.0$  and  $10 \text{ cm}^2\text{V}^{-1}\text{s}^{-1}$  respectively, for a concentration in the range  $10^{19}-10^{21} \text{ cm}^{-3}$ . The thermal conductivity is assumed to be given by  $\lambda = \lambda_L + L\sigma T$ , with  $L = 1.5 \times 10^{-8}$ .  $\lambda_L$  is normally taken to be  $10\text{mW}/\text{cm deg}$ , and it can be seen that the "target" of  $\bar{Z} = 1$  is attained only if  $\mu > 1 \text{ cm}^2\text{V}^{-1}\text{s}^{-1}$ , at the higher carrier concentrations. An increase in  $\lambda_L$  to  $50\text{mW}/\text{cm deg}$  makes the goal of  $\bar{Z} = 1$  difficult to attain. The specifications that  $\mu > 1 \text{ cm}^2\text{V}^{-1}\text{s}^{-1}$  and  $\lambda_L \lesssim .01 \text{ W}/\text{cm deg}$  are difficult to meet over a wide range of temperature.

A central problem in the materials engineering of an appropriate composition is that the requirement of a low lattice thermal conductivity implies a complex crystal structure, and this favors the formation of small polarons and hence a low carrier mobility. The tendency for small polaron formation also depends on the lattice polarization (the difference between static and dynamic dielectric constant), the electron-lattice coupling, the degree of disorder and the inter-site jump distance. There is little hard data on which the choice of a high-boron compound with relatively high mobility could be based, although Golikova (36) has argued that  $\beta$ -boron should not be considered a small-polaron conductor but should be described as a quasi-amorphous material because of a high degree of disorder. There

ORIGINAL PAPER  
OF POOR QUALITY

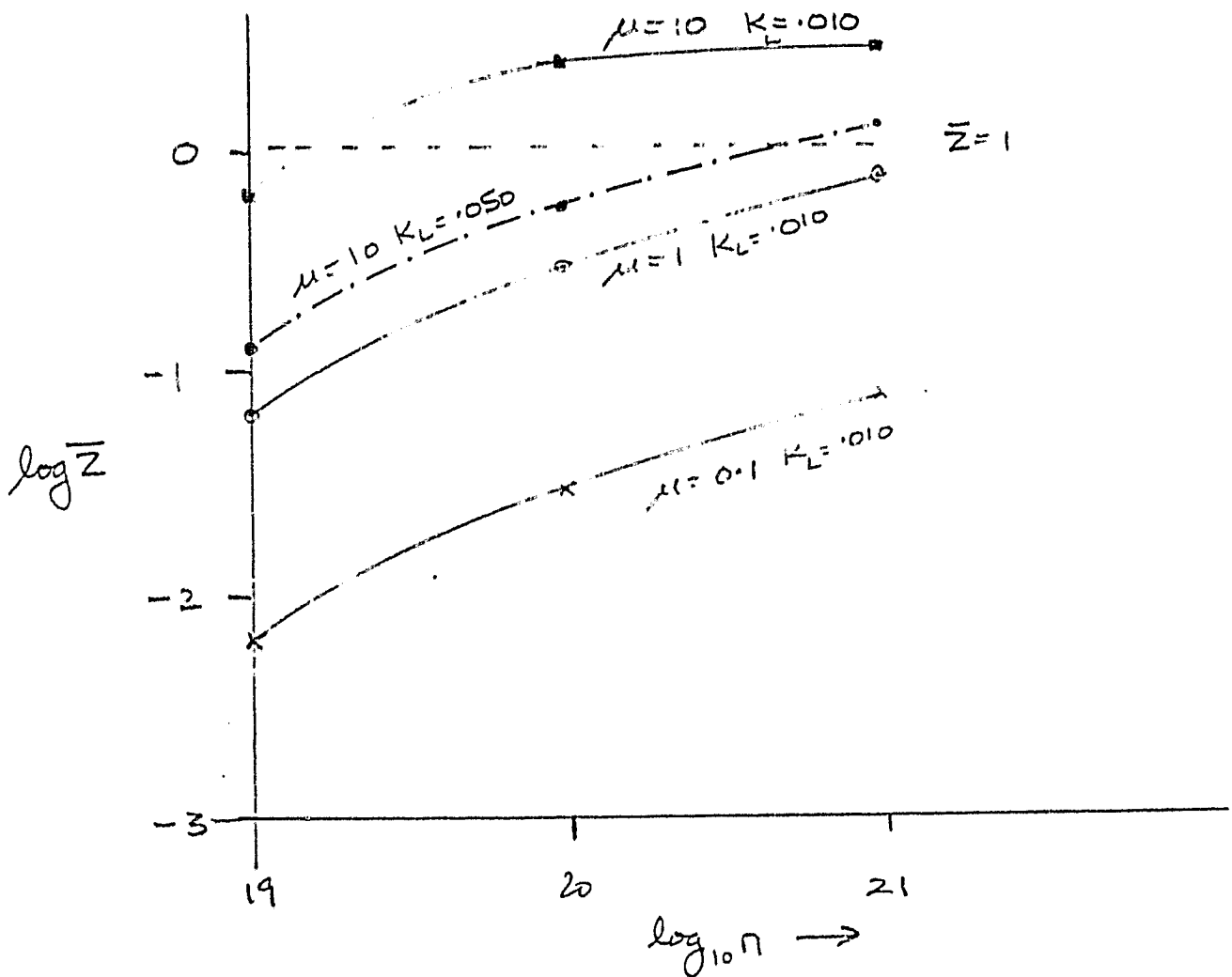


Fig. 8. Figure of merit  $\bar{Z}$  versus carrier concentration for various values of mobility  $\mu$  ( $\text{cm}^2 \text{V}^{-1} \text{s}^{-1}$ ) and lattice thermal conductivity ( $\text{W cm}^{-1} \text{deg}^{-1}$ ).

is strong evidence [see ref (36)] for the existence of a high concentration of traps, presumably associated with some physical defects rather than with chemical impurities, and we hope to be able to throw some light on the nature of the defects in  $\beta$ -boron and related materials once crystals of suitable quality are available.

One experimental test which appeared to us to be potentially very valuable for characterization of materials involves the measurement of the activation energy of the mobility. Ideally the drift mobility should be measured directly as a function of temperature but this is a difficult experiment if reliable results are to be obtained. In our previous report, we suggested the use of the parameter  $Q$ , defined by

$$Q = e\alpha/k + \ln\sigma \quad (9)$$

which is expected to be independent of temperature for a conventional semiconductor in which  $\alpha$  decreases with  $T$  and  $\ln\sigma$  increases with the same activation energy. In materials exhibiting hopping behavior, it is sometimes observed that  $\alpha$  is independent of temperature so that  $Q$  gives the activation energy of the mobility. The complicating factor which makes  $Q$  less useful is the increase in  $\alpha$  with  $T$  for semiconductors in which carriers hop between inequivalent sites.

As shown in Fig. 9, both of the leading candidate materials show an increase in  $\alpha$  with  $T$ , although this is presently supposed to be for different reasons - small polaron hopping between inequivalent sites in the case of  $B_{13}C_2$ , and "metallic" behavior in the case of  $LaS_{1.4}$ . The different types of behavior are reflected in the decrease in  $\sigma$  with  $T$  in the case of  $LaS_{1.4}$  compared with the normal increase (for a semiconducting material) in the case of  $B_{13}C_2$ . The large contribution of the 'A' term to the Seebeck coefficient of  $B_{13}C_2$  and similar materials is a very useful factor which was underestimated in the plots of Fig. 7. The disadvantage with most of these materials is that the decrease in  $\alpha$  compounds the fall in  $\bar{Z}$  due to the decrease in  $\sigma$  at lower temperatures. It is clearly very desirable to obtain a better understanding of the dominant sites in the boron or ' $B_4C$ ' lattice between which hopping occurs, so that this contribution to the Seebeck coefficient can be better controlled.

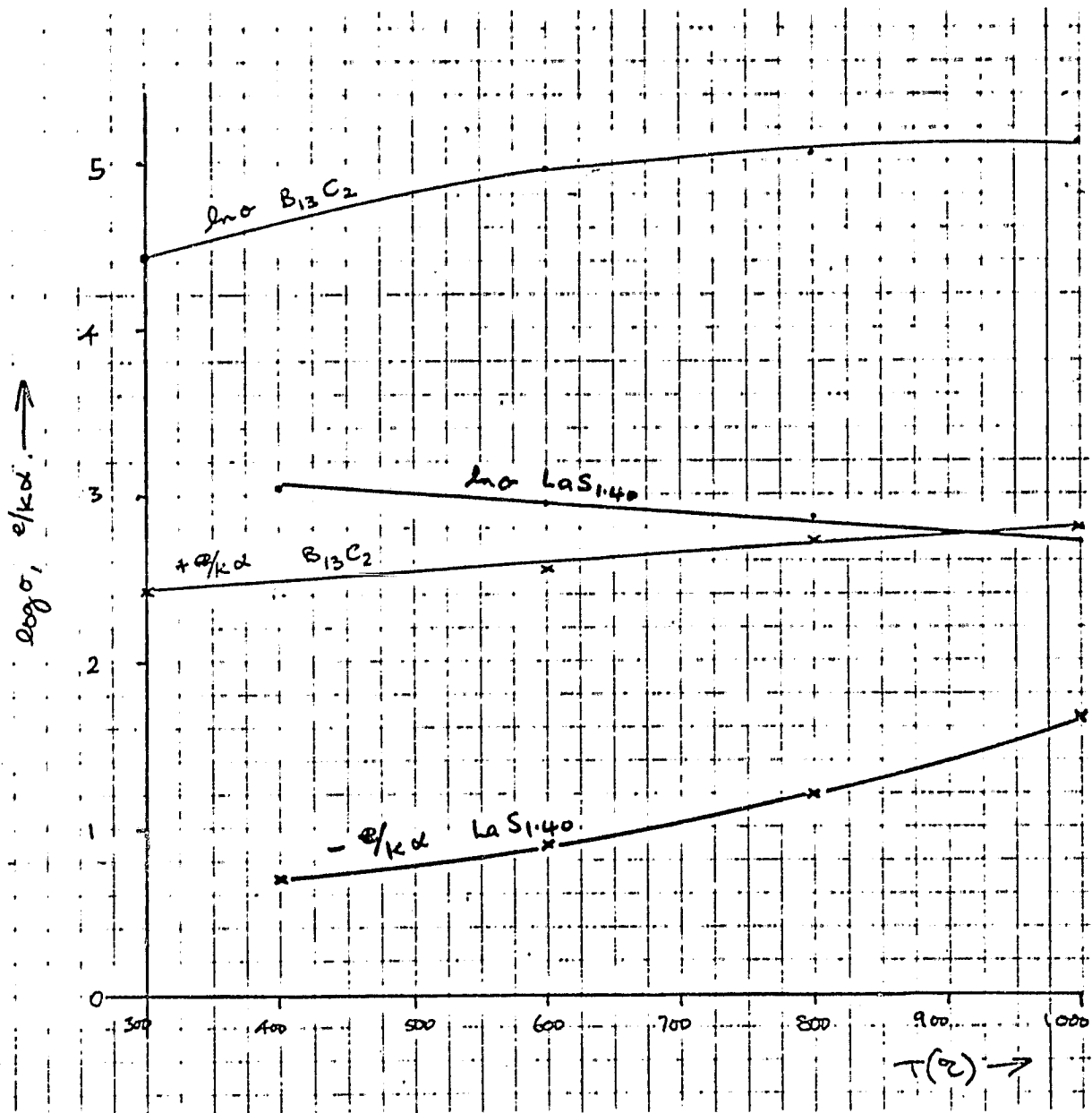


Fig. 9. Temperature dependence of electrical conductivity  $\sigma$  and  $e_a/K$  for boron carbide and lanthanum sulphide.

### III. EXPERIMENTAL

#### A. NEW APPARATUS

During the past year our capability to prepare polycrystalline samples and to make electrical measurements has greatly increased with the purchase of a hot pressing furnace and the construction of apparatus for Seebeck/electrical conductivity measurements and for Hall effect measurements. These facilities will be briefly described.

##### 1. Hot Press

The Astro HP20 hot pressing furnace has a 10,000 kg frame and a graphite furnace with a maximum operating temperature of 2500°C. It allows operation with an inert atmosphere or vacuum. A control system allows programming both of the temperature and pressure cycle, and a ram position indicator gives a continuous display of the compression. We have used high strength graphite die sets, the lower plunger being of 1/2" diameter, the upper of 3/8" diameter, with a machined hot-pressed BN liner. BN end caps were also used, and samples of 3/8"-1/2" length fabricated.

##### 2. Seebeck Apparatus

Apparatus based closely on the "small gradient" apparatus described by Zoltan (37) has been constructed and is shown in Fig. 10. The sample is mounted between Mo contacts and pressure is adjusted by steel springs outside the furnace chamber. Holes are drilled into the sample using 0.75 mm diamond-tipped drills and Nb/W thermocouples are inserted into these holes and held there by molybdenum wire plugs, the end region of the couple being bent back to generate some lateral tension. A single subsidiary heater is used to produce a temperature gradient. The furnace is of Mo wire held by Ceramabond 503 cement, and is insulated by 10 layers of dimpled tantalum sheet. The furnace case is of stainless steel and is located in a Varian HS-2 vacuum system capable of pressures below  $10^{-6}$  torr.

##### 3. Hall Effect

A Hall effect apparatus was built to the design of Lupu et al

ORIGINAL SOURCE  
OF POOR QUALITY

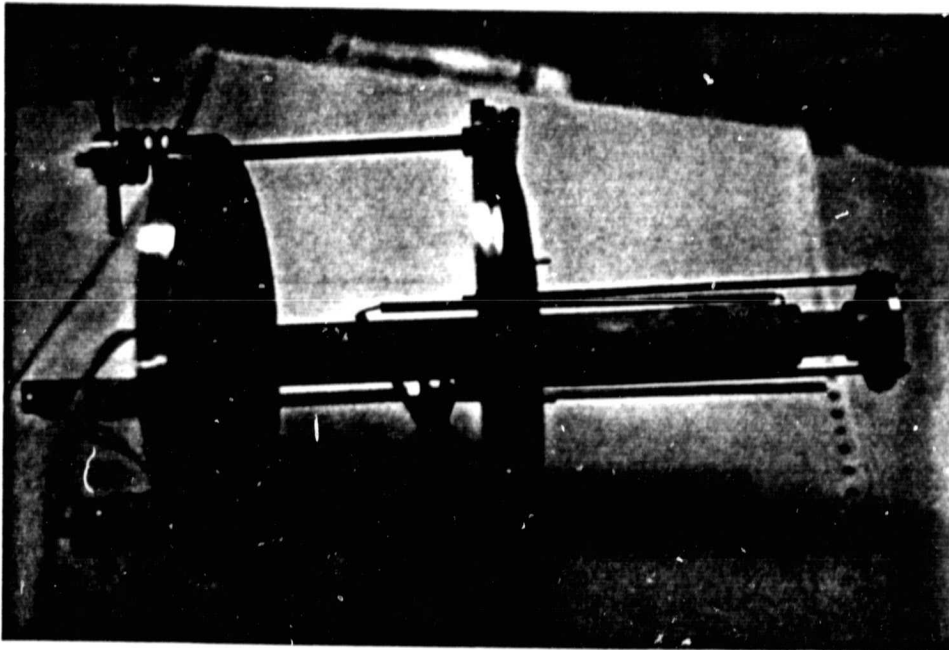


Fig. 10. Sample holder for Seebeck coefficient measurement.

(38). This is based on lock-in amplifier detection of the Hall signal in the  $10^2$ - $10^3$  Hz frequency range. This apparatus was built by a visiting scholar, Prof. D. S. Tannhauser from the Technion, Israel, who is very experienced with AC Hall measurements (39, 40). A novel source/detector system with improved characteristics was built to the design of Friend & Bett (41). This scheme uses two fixed voltage probes, with the Hall current divided on one side between a pair of contacts in order to balance the current flow and give zero output in the absence of the magnetic field. In principle an AC system offers the advantage of greater sensitivity over DC methods for samples of low Hall mobility. Construction of the apparatus is complete, but time was not available for test measurements before Dr. Tannhauser's departure and we have been unable to transfer any manpower from other parts of the program.

#### B. SILICON BORIDES

As stated earlier, the silicon borides appear to be a possible alternative to boron carbides as p-type refractory thermoelectrics. The Si-B system has three well-established phases: the  $\beta$ -boron solid solution,  $\text{SiB}_6$  and  $\text{SiB}_4$ . The solubility of silicon in  $\beta$ -boron has been reported to extend up to a composition  $\text{SiB}_{14}$  (42), and this is the composition reported on by Pistoulet and co-workers (28). Silicon hexaboride  $\text{SiB}_6$  is orthorhombic (43) with  $a = 14.346 \text{ \AA}$ ,  $b = 18.226 \text{ \AA}$  and  $c = 9.848 \text{ \AA}$ , and has 300 atoms in the unit cell distributed among 5 crystallographically independent polyhedra and 24 interstitial atoms.  $\text{SiB}_4$  is isostructural with  $\text{CB}_4$  and also has a wide homogeneity range, from  $\text{SiB}_{2.8}$  -  $\text{SiB}_{4.0}$ .  $\text{SiB}_4$  is unstable above  $1270^\circ\text{C}$ . In addition to these fairly well-established phases, Nowotny et al (44) reported an  $\text{SiB}_{12}$  phase isomorphous with  $\text{AlB}_{12}$ , and recently Malé and Salanoubat (45) reported an " $\text{SiB}_n$ " phase with  $n \sim 24$ . Of particular interest for thermoelectric applications is the report by Djafarov et al (46) that a composition  $\text{SiB}_9$  had a carrier mobility of  $15\text{-}70 \text{ cm}^2/\text{Vs}$ .

In view of these complexities, we considered it essential to carry out a careful investigation of the Si-B phase diagram in the range from SiB<sub>6</sub> to  $\beta$ -boron. Mixtures of Si and B powders were well mixed and heated for at least 1 hr at 1650°C in an argon atmosphere. The resulting samples were analyzed using x-ray diffraction to determine the phases present, and the results are shown in Fig. 11 on the composite phase diagram put together by Elliot (47) from three investigations. Samples with less than 10 wt % Si showed only the  $\beta$ -boron phase, while SiB<sub>6</sub> could be detected in the sample with 12.5 wt % Si. Samples between this latter composition and 30 wt % Si (SiB<sub>6</sub>) showed only the two phases SiB<sub>6</sub> and  $\beta$ -B(ss). We therefore conclude that separate phases SiB<sub>9</sub>, SiB<sub>12</sub> and "SiB<sub>n</sub>" do not exist, in equilibrium at 1650°C. This finding is in agreement with a similar study by Viala and Bouix (48). The limiting solubility of silicon in  $\beta$ -boron can be determined most accurately by plotting the 'a' lattice constant versus silicon concentration (Fig. 12). Our data is plotted together with that of Viala and Bouix and of Malé and Salanoubat, and these clearly show a limiting solubility of  $5.6 \pm 0.3$  at % Si, corresponding to a composition SiB<sub>17</sub>. This limiting composition is expected to be temperature dependent and a value of SiB<sub>14</sub> at 1250°C (28) seems reasonable, although this seems to have been selected with reference to Giese's work (on a sample prepared by cooling from Si solution at higher temperature) rather than being determined experimentally.

In the course of characterizing Si-B samples made in various ways, we noted that microhardness is a simple and fairly reliable means of distinguishing silicon, SiB<sub>6</sub> and  $\beta$ -boron. We measured Knoop hardness values of around 1040 kg/mm<sup>2</sup> for Si, 2400-3000 for SiB<sub>6</sub>, and 3080-3500 for SiB<sub>17</sub>. The actual data for representative samples is listed in Table 4 together with some literature values for the Knoop hardness. Our values are consistent with these earlier measurements except that the value for  $\beta$ B (ss) is higher than that reported for  $\beta$ -boron by Cline (43).

ORIGINAL PAPER  
OF POOR QUALITY

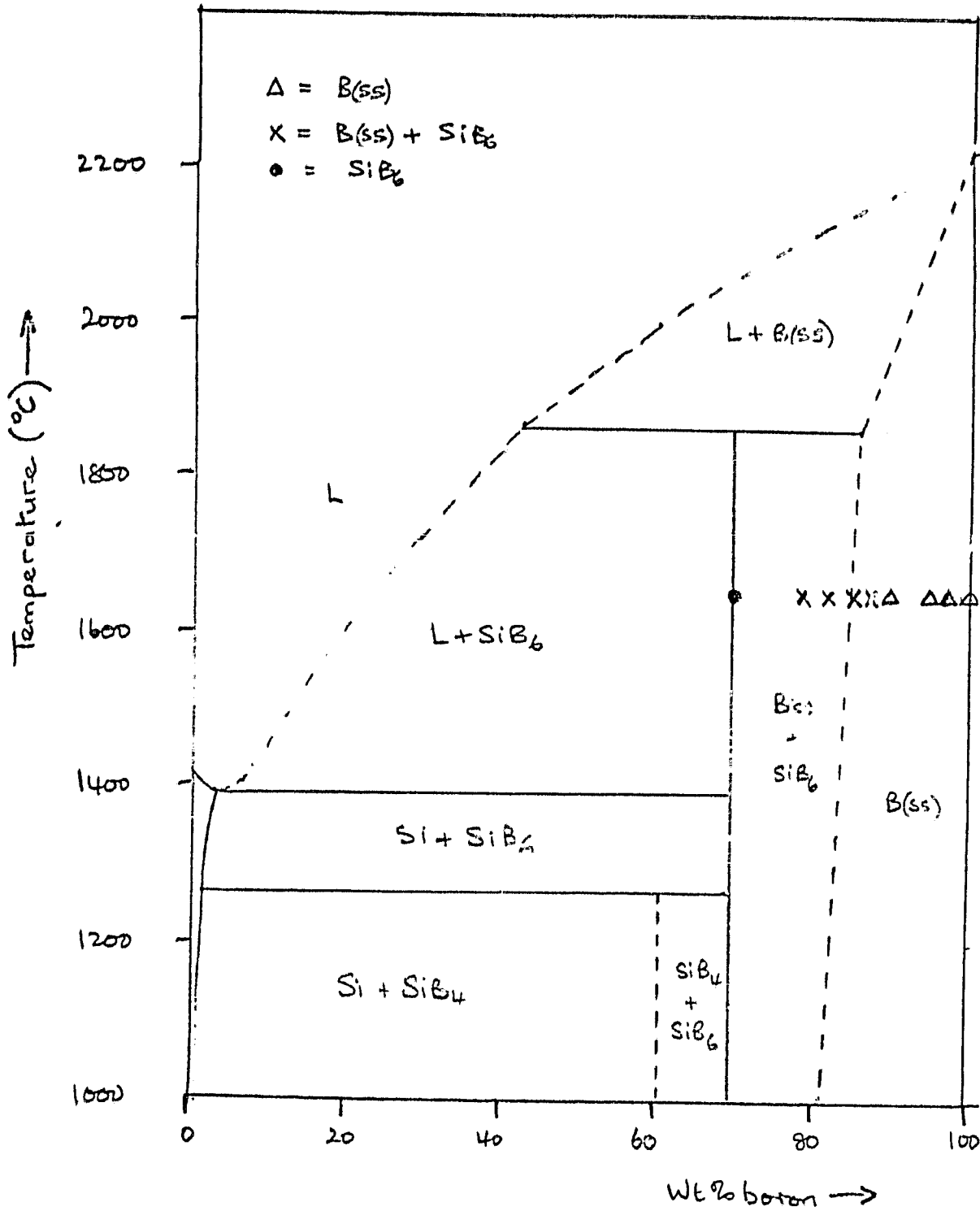


Fig. 11. Si-B phase diagram with our analytical data for 1650°C isothermal section.

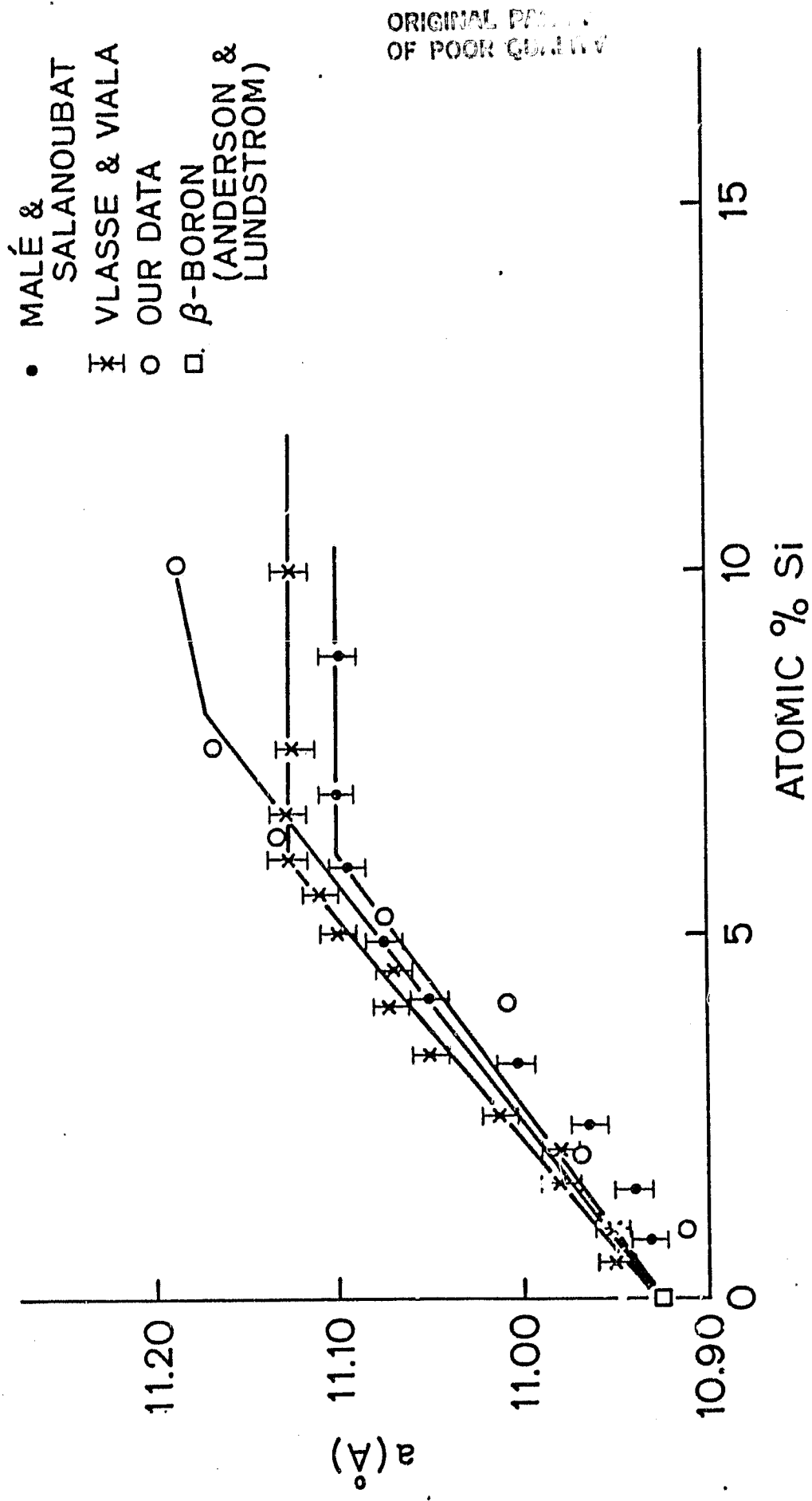


Fig. 12. Lattice parameter a for β-boron versus concentration of Si.

Table 4: Microhardness Data

<u>SiB Ratio</u>	<u>X-Ray Analysis</u>	<u>Knoop Hardness (kg/mm<sup>2</sup>)</u>
1:6	SiB <sub>6</sub> + Si	2470 - 2940 1040 ± 50
1:7.5	SiB <sub>6</sub> + Si	2390 - 2800 1040 ± 50
1:7.5	SiB <sub>6</sub> + Si	2800 - 3000 1040 ± 50
1:8	SiB <sub>14</sub>	3080 - 3500

<u>Literature Data</u>	<u>Knoop Hardness (kg/mm<sup>2</sup>)</u>	<u>Reference</u>
SiB <sub>4</sub>	1955 - 2120	Feigelson & Kingery
SiB <sub>6</sub>	2300 - 2400	Feigelson & Kingery
SiB <sub>6</sub>	1900 - 2400	Colton
SiB <sub>6</sub>	1740 - 2050	Cline
SiB <sub>n</sub> > 10	2750 ± 70	Powell
Si	1000	Runyan
B	1940 - 2630	Cline

A number of attempts were made to synthesize samples of boron-silicon materials using cold pressing followed by reaction sintering. These were generally unsuccessful, and so our more recent work has been concentrated on hot-pressing. A range of samples from  $\beta$ -boron to  $\text{SiB}_6$  was pressed at 6000 psi in purified argon for 1 hr and the results are shown in Table 5. The results of x-ray analysis are consistent with the earlier data on loose powders, although small traces of a second phase could be detected metallographically in samples which appeared to be single phase according to the x-ray data. This problem was attributed to imperfect mixing. The major problem was that of obtaining samples of high density. Samples of  $\text{SiB}_6$  prepared at 1500°C and 1600°C showed poor density (about 89% of theoretical), but the sample density increased to a value close to theoretical (2.44 g/cm<sup>3</sup>, compared with 2.40-2.49 g/cm<sup>3</sup> reported in the literature) when the pressing temperature was increased to 1780°C.  $\beta$ -boron samples prepared at 1600°C also showed high porosity (about 72% of theoretical density).

Hot pressing at 1780°C therefore appears to be required in order to achieve acceptable density, but it also leads to problems of carbon contamination and decomposition of the  $\text{SiB}_6$  through loss of Si by evaporation. This was revealed by traces of extra  $\text{B}_4\text{C}$  lines in the x-ray diffraction pattern of the  $\text{SiB}_6$  sample fired for 1 hour. When a similar sample was fired for 3 hours, the surface became extremely brittle so that a Vickers hardness measurement could not be made.

The problem of carbon contamination has become more apparent in a recent series of experiments using Group II dopants (Mg, Ca, Sr, Ba) in  $\beta$ -boron. Carbon incorporation can, however, be much reduced if samples are pressed below 1700°C. A series of  $\text{SiB}_6$  samples was deliberately carbon doped, and good densities were achieved by pressing for 3 hours at 1700°C. The  $\text{SiB}_6$  structure appears to dissolve carbon up to 9%, with little change in the unit cell dimension, as can be seen from the series of x-ray diffraction patterns shown in Fig. 13.

Table 5: Hot-Pressed Si-B Samples

<u>At % Si</u>	<u>T</u> °C	<u>X-Ray Analysis</u>	<u>Density</u> (g/cm <sup>3</sup> )	<u>Knoop Hardness</u> (kg/mm <sup>2</sup> )
14.3	1500	SiB <sub>6</sub>	2.18	2100
14.3	1600	SiB <sub>6</sub>	2.08	2100
14.3	1780	SiB <sub>6</sub> + ?	2.44	>2200
14.3	1780*	SiB <sub>6</sub> + Bss	2.43	-
11.8	1600	SiB <sub>6</sub>	-	2100
10.0	1600	SiB <sub>6</sub> + Bss	2.12	2200/3500
7.4	1600	SiB <sub>6</sub> + Bss	2.12	2500
5.9	1600	Bss	2.07	2400
4.8	1600	Bss	1.98	2400
2.4	1600	Bss	1.66	2400-2900
0	1600	Bss	1.69	>2500 (brittle)

\*Sample fired for three hours.

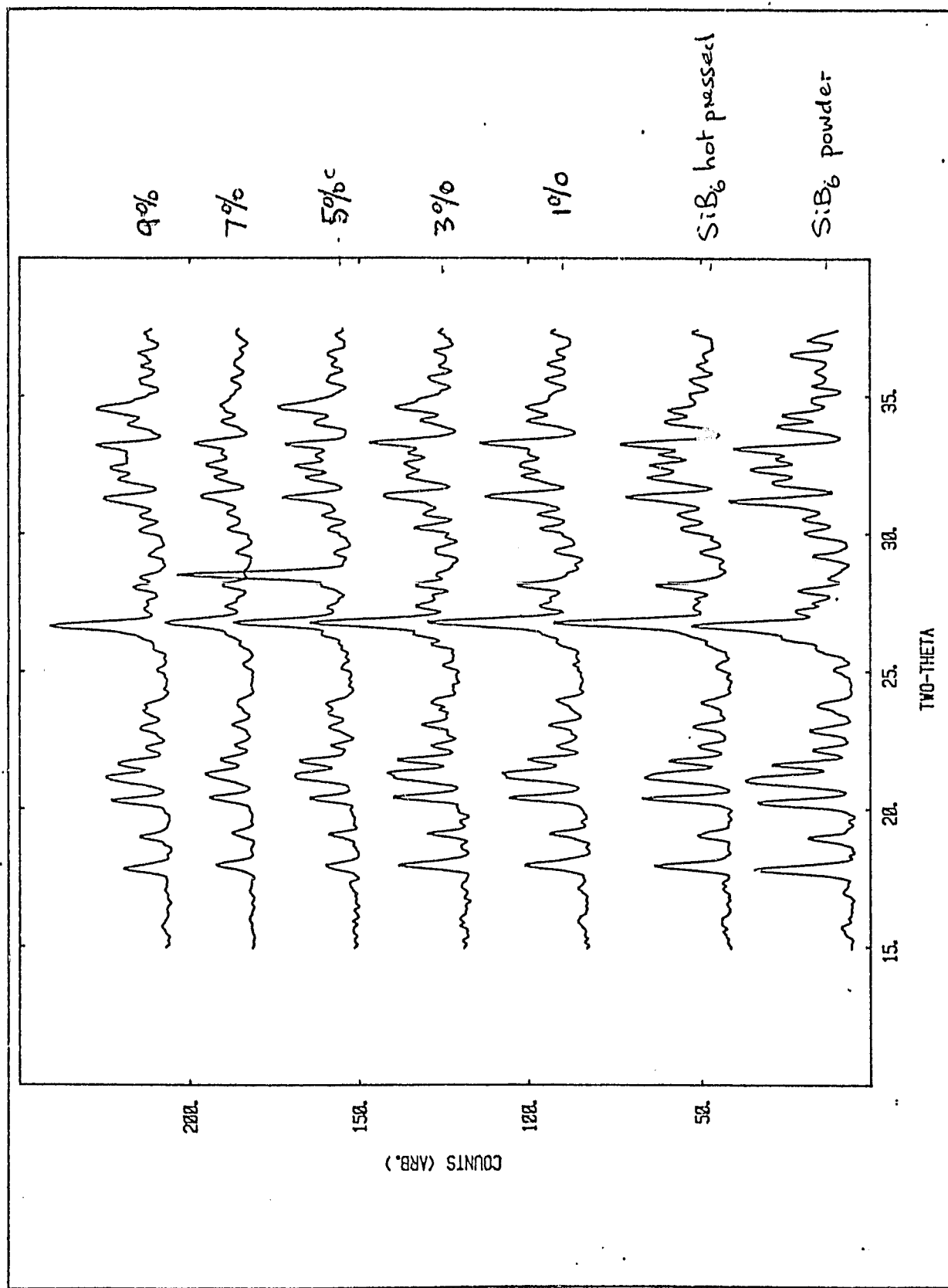


Fig. 13. X-ray powder diffraction pattern for SiB<sub>6</sub> and carbon-doped samples.

## B. SINGLE CRYSTAL GROWTH

Single crystals of silicon borides and boron carbides are very desirable for an improved understanding of the mechanism of electrical conduction in these materials. Since hot-pressing tends to produce fine-grain materials, it is not clear that measured properties are not dominated by grain-boundary effects. Porosity and compositional inhomogeneity are related problems which could influence the data. In addition, most successful electronic devices use single crystal material and it may be that the performance of high temperature thermoelectric generators would be much improved if the elements were fabricated from single crystals. This point was made by Israeli researchers (49) at the 1983 Conference on Thermoelectric Energy Conversion. Mainly because of the potential contribution of single crystals to the understanding of high-boron materials, we have investigated a number of methods to prepare single crystals large enough for Seebeck measurements.

### 1. Si-B Binary System

The simplest method in principle to grow crystals of  $\text{SiB}_6$  and  $\text{SiB}_{17}$  involves slow cooling of appropriate compositions in the Si-B binary system. From the phase diagram (Fig. 11) compositions containing more than 42 wt % boron at temperatures above  $1870^\circ\text{C}$  are expected to yield the  $\beta$ -boron solid solution while more silicon-rich compositions at lower temperatures should yield  $\text{SiB}_6$ . We have performed a total of 14 experiments in which Si/B melts in BN crucibles were cooled in an Astro furnace using programmed cooling at rates normally around  $25^\circ\text{C/hr}$ . The starting temperature was in the range from  $1720^\circ\text{C}$  to  $2100^\circ\text{C}$ .

Three major problems are experienced. First, the silicon tends to evaporate rather than react, and the volatilization rate even from a fully reacted melt is relatively high. Second, in a partially reacted melt the boron tends to float, even though the room temperature density of  $\beta$ -boron ( $2.35 \text{ g/cm}^3$ ) is higher than that of silicon ( $2.33 \text{ g/cm}^3$ ). This tendency to separate increases the problem

of fully reacting the melt prior to cooling. Third, it is very difficult to separate the crystals from the matrix after cooling to room temperature because of the chemical similarity of  $\text{SiB}_6$  (or  $\text{SiB}_{17}$ ) and silicon.

It was found that the weight loss during reaction of the Si and B starting materials could be minimized if the charge was held for several hours at a temperature just above the melting point of silicon. Amorphous boron (Callery Co.) was found to be more reactive than the coarser-grained material from Alfa Ventron. However, silicon evaporation was significant even when pre-reacted  $\text{SiB}_6$  (Cerac) was used, and remained troublesome even when a lidded crucible was used or when a BN cap was floated on the top of the melt. The solution wets BN and so the solution tends to creep out of the crucible in addition to its loss in the vapor phase.

Small crystals of  $\text{SiB}_6$  and  $\text{SiB}_{17}$  were produced in these experiments, always embedded in a dense matrix of solidified solution. Attempts were made to separate crystals using the method suggested by Feigelson and Kingery (50). The sample is placed in a 25% HF solution, and concentrated nitric acid added drop by drop to control the reaction rate. Cooling is required to prevent the exothermic reaction from producing temperatures at which the boride dissolves rapidly. Even with this precaution, however, it was not found possible to isolate crystals large enough for Seebeck and conductivity measurements.

## 2. Growth from Copper Solution

Metal solutions offer the possibility of crystal growth over a range of temperatures and rather large crystals of some borides have been grown particularly from aluminum solutions. Bouchacourt and Thevenot (51) grew small crystals of  $\text{SiB}_4$  by rapid cooling of a solution of Si and B in copper, but the use of aluminum solutions yielded aluminum borides. Tin, another widely used metallic solvent for crystal growth, is reported not to react with boron so we restricted our investigation to Cu solutions. Bouchacourt and

Thevenot used a composition 33% Cu + 33% B + 33% Si, contained in alumina crucibles and melted in an rf furnace and cooled very rapidly to yield crystals a few hundred  $\mu\text{m}$  in size. Initially we concentrated on solutions with much higher Cu concentrations, growing from maximum temperatures of around  $1450^\circ\text{C}$ . As in the case of the Si-B melts, it was initially found difficult to produce a fully reacted melt, but a considerable improvement was noted when Callery amorphous boron was substituted for Alfa coarsely powdered material. The first crystals of mm size were obtained by programmed cooling a melt containing 200 g Cu + 2.4 g Si + 6 g B at  $8^\circ\text{C}/\text{hr}$  from  $1400^\circ\text{C}$ . These crystals were found to contain significant amounts of aluminum and had a typical composition  $\text{Al}_3\text{Cu}_2\text{Si}_{0.1}\text{B}_{94.9}$ . The aluminum problem was removed by replacing the alumina crucibles with boron nitride crucibles machined from hot-pressed rods.

In all cases of crystals grown from relatively dilute solution, the crystals grow on the crucible walls and on the melt surface (see Fig. 14a), and are of 1-2 mm size (Fig. 14b). It is a general principle of high temperature solution growth that a high solute concentration is a favorable factor in improving crystal size and quality. Experiments in which the size and number of crystals grown is similar to that shown in Fig. 14 have been performed with copper concentrations in the approximate range 70-95%. The copper-rich matrix is soluble in nitric acid and so it is relatively easy to separate the crystals after growth. This procedure of dissolving the matrix becomes more difficult, however, as the silicon content in the melt increases.

Experiments were also performed with melts containing relatively low copper concentrations, in the range 10-30%. The temperatures required for dissolution of the boron are then  $1600$ - $1850^\circ\text{C}$ . Well-faceted crystals 1-2 mm in size are also produced in slow-cooling experiments, but these are in general difficult to remove from the matrix. One crystal grown from a melt of composition (by weight) 10% Cu + 27% Si + 63% B was powdered and found to give an x-ray pattern in agreement with that expected for  $\text{SiB}_6$ , except that



additional peaks due to Si and  $\beta$ -boron could be detected.

The problem of separating the crystals from the melt is being attacked by the use of a "cold finger", a rod of BN 3mm in diameter inserted 1-2 mm into the top of the melt and slowly pulled and rotated during programmed cooling. A small axial hole is drilled into the end of the rod to encourage the nucleation of a single crystal at the end of the rod. In experiments to date, however, the material grown on the end of the rod has been polycrystalline. The present series of experiments is aimed at optimizing the growth conditions using this cold finger technique.

### 3. Fiber Crystal Growth

Early experiments were described in our previous reports which were aimed at growing single crystals of  $\text{SiB}_6$  and boron carbides in the form of fibers about 0.2-0.3 mm in diameter and a few cm long. The method used is a laser-heated pedestal technique in which a hot-pressed source rod typically 1 mm in diameter and over 1 cm long is melted at the end by radiation from a 50 w  $\text{CO}_2$  laser. The molten region is contacted by a seed or wire which is then pulled at a fairly rapid rate ( $\sim$  mm/min) while the source rod is also moved to maintain the supply of material to the molten zone.

$\text{SiB}_6$  is a rather difficult material to grow by this technique since it melts incongruently and there is a large difference in composition between the liquid and solid phase in the temperature region where the  $\text{SiB}_6$  is the stable phase (about  $1400^\circ\text{C} - 1850^\circ\text{C}$ ). The growth of fibers of incongruently melting materials has been achieved with our apparatus, notably in the case of yttrium iron garnet, a necessary condition being that the growth rate must be slowed down to allow solute diffusion through the liquid zone. Silicon evaporation is troublesome when attempts are made to grow  $\text{SiB}_6$  from temperatures near the upper end of its stability range. The difficulty with growth from the lower end of the range is the high reflectivity of molten silicon, which reduces the coupling of energy from the laser beam so that a molten zone cannot be maintained. It

is, in fact, very difficult to melt silicon with our apparatus in spite of its low melting point ( $1415^{\circ}\text{C}$ ) in comparison with refractory oxides and other materials which can be melted easily.

In the case of the boron carbides, volatilization is not a problem but their liquidus temperatures are much higher and we have again found it difficult to melt the end of the source rod and to control the molten zone. Initial experiments with  $\text{B}_4\text{C}$  utilized source rods about 1 mm in diameter and of square cross section, which were cut (with difficulty) from hot-pressed samples supplied by GA. It was found to be preferable to use smaller diameter rods, and cylindrical rods of about 0.5 mm diameter were fabricated on a centerless grinder. Careful machining was found to be very important since the source rod is rotated in the laser beam to minimize the temperature asymmetry resulting from non-uniform heating, and any irregularity in the source rod can cause serious temperature variations if the tip of the rod moves radially as the rod rotates.

Even with small diameter, ground rods it was not found possible to control a molten zone between source and seed rods with sufficient precision to grow a fiber. Recently a breakthrough was achieved by the use of a reflecting sphere surrounding the sample but with holes to permit entry of the beam. Also, the direction of growth was reversed, the fiber being grown downwards. With these modifications the crystal shown in Fig. 15 was grown. This is 2 mm long and 0.35 mm in diameter, and is long enough to allow measurements of electrical conductivity, at least by a two-terminal method. Its morphology is, however, very rough because of irregular growth ridges, and we hope to grow greatly improved crystals in the near future.

### C. ELECTRICAL MEASUREMENTS

Electrical conductivity and Seebeck data from  $500^{\circ}\text{C}$ – $1000^{\circ}\text{C}$  on a sample of  $\text{SiB}_6$  of 90% density, are shown in Fig. 16. The Seebeck coefficient was found to be in the range from 250 to 300  $\mu\text{V}/\text{deg}$  with a maximum around  $750^{\circ}\text{C}$ . No  $\text{SiB}_6$  Seebeck data is available in the literature for comparison. The electrical conductivity of our sample

OF POINT



Fig. 15. Fiber crystal of B<sub>9</sub>C grown by laser-heated pedestal method.

ORIGINAL PAPER  
OF POOR QUALITY

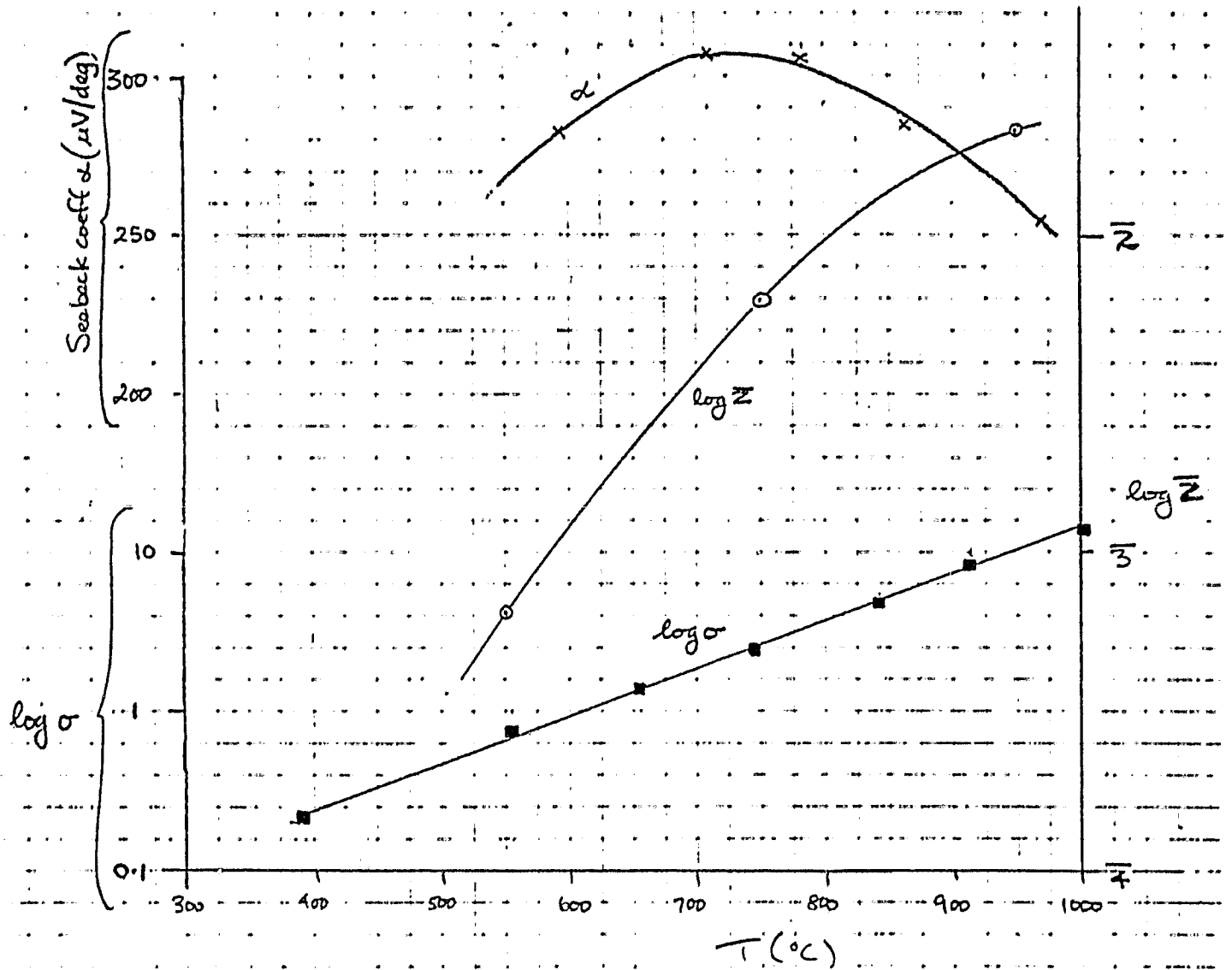


Fig. 16. Electrical conductivity  $\sigma$ , Seebeck coefficient  $\alpha$  and figure of merit  $\bar{Z}$  for hot-pressed  $\text{SiB}_6$ .

varied from about 10 ohm cm to 0.2 ohm cm in this temperature range and is an order of magnitude lower than that reported by Feigelson and Kingery (50). Part of this discrepancy is due to the fact that our data are uncorrected for sample porosity, and this correction would increase our values by about 20%. Micrographic examination revealed small traces of a second phase in our sample, and the presence of  $\beta$ -boron would also be expected to lower the conductivity. An unusual feature of our data is the observation that  $\log \sigma$  versus  $T$  is linear over the range of measurement, which implies that a plot of  $\log \sigma$  versus  $1/T$  has pronounced curvature. We also plotted  $\log \sigma T^{3/2}$  versus  $1/T$  since similar plots for boron carbides are linear (52). This latter plot is much more linear than  $\log \sigma$  vs  $1/T$ , but still exhibits significant curvature.

In Fig. 17 the figure of merit  $\bar{Z}(=ZT)$  for  $\text{SiB}_6$  is compared with that of  $\text{SiB}_{14}$  and  $\text{SiB}_4$ . The  $\text{SiB}_{14}$  data are the best plots from the work of Pistoulet et al (28) and shows  $\bar{Z}$  approaching unity as  $T \rightarrow 1000^\circ\text{C}$ . The data for  $\text{SiB}_4$  is for a Cerac sample which was hot-pressed by Syncal during the early days of the Stanford-Syncal collaboration. Thermal conductivity data is from Feigelson and Kingery (50). This sample shows a higher figure of merit than  $\text{SiB}_{14}$  at the lower temperatures but  $\bar{Z}$  appears to level off at a value not much above  $10^{-2}$ . Our data for the  $\text{SiB}_6$  sample compares favorably with  $\text{SiB}_4$  at the higher temperatures, but  $\bar{Z}$  is an order of magnitude lower than that of  $\text{SiB}_{14}$ . However, to match the  $\text{SiB}_{14}$  figure we need only increase the electrical conductivity to the Feigelson/Kingery value, and it must be recalled that the  $\text{SiB}_{14}$  data is the best of a relatively long investigation.

Carbon has been added to  $\text{SiB}_6$  in an attempt to increase the electrical conductivity. Carbon appears to dissolve in the  $\text{SiB}_6$  lattice up to at least 5%, and the electrical conductivity of this 5% doped sample is higher than that of undoped  $\text{SiB}_6$  by a factor of about 3. The influence of impurities on this data is still uncertain. According to fusion analyses by Oremet, Alfa boron contains about 0.4 wt% carbon and 0.3-0.7 wt% oxygen, while Callery amorphous boron

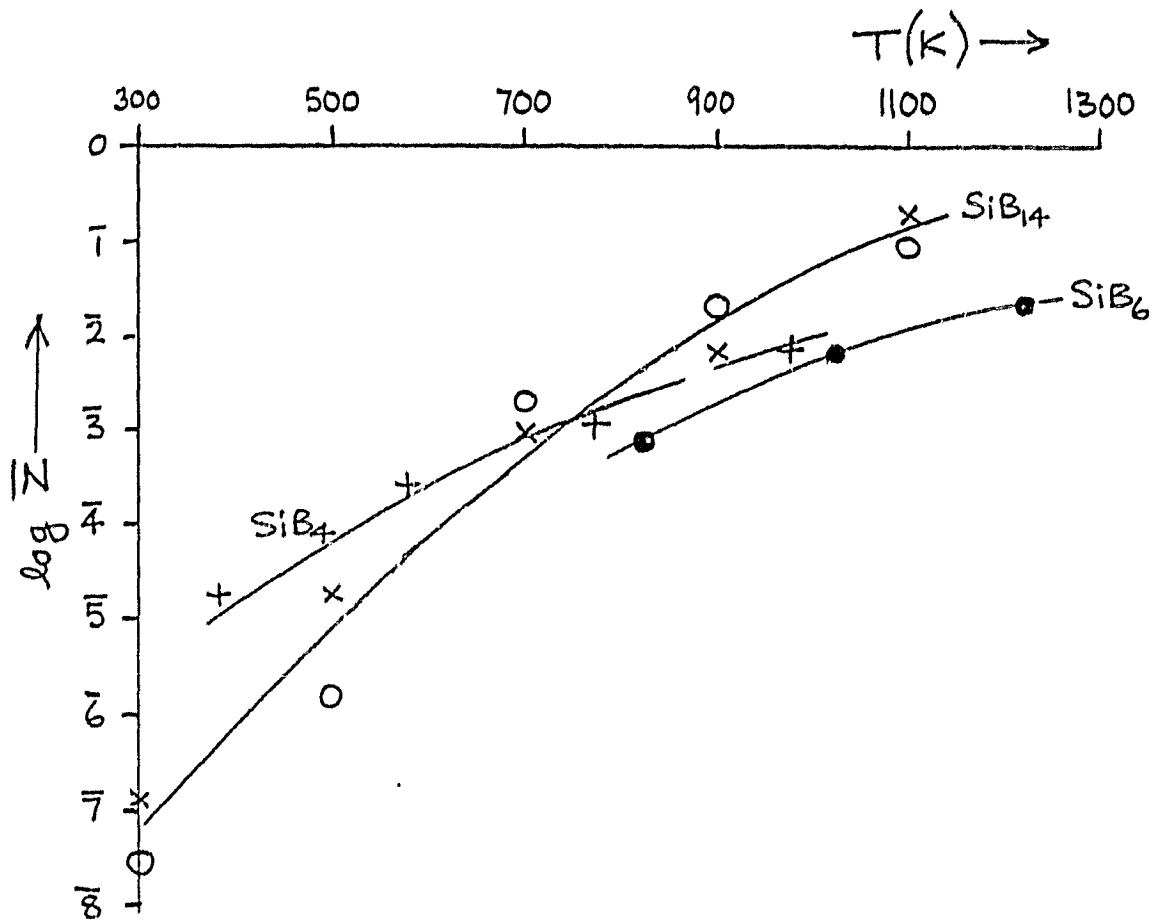


Fig. 17. Figure of merit of SiB<sub>6</sub> compared with SiB<sub>4</sub> (Stanford-Syncal) and SiB<sub>4</sub> (Pistoulet).

contains less than  $10^{-3}$  wt% carbon but 1.5 wt% oxygen. The Gallery material seems preferable if the oxygen can be removed as  $B_2O_3$  by evaporation under vacuum at about  $1800^\circ C$ . We have, however, found that hot pressing at this temperature in our furnace can lead to severe carbon contamination. Cerac  $SiB_6$  contains .26 wt% carbon, and 2.5 wt% oxygen, in addition to  $\sim 1\%$  of Ca and Mg, so is unsuitable for serious studies.

#### IV. FUTURE PLANS

In the much reduced program of the coming year, we plan to concentrate on three main areas: Fundamental studies aimed at advancing the level of understanding of the mechanisms and particularly at predicting compositions of high figure-of-merit; a strong emphasis will be placed on crystal growth of important candidate materials and measurements of the Seebeck coefficient and electrical conductivity of the single crystals produced. Studies of dopant incorporation in  $SiB_6$  and their influence on its electrical properties will also be continued. The elimination of unwanted impurity effects is an important aspect of the latter investigation.

Fundamental studies, particularly of the high-boron semiconductors, are of great importance particularly because of the complexity of these materials. Problems such as the low mobility at fairly low temperatures are unlikely to be solved in the absence of a firm understanding of the electrical conduction mechanism. Measurements on single crystals could be particularly valuable since they avoid grain boundary effects and allow us to study anisotropic effects which are very important to our understanding of these complex materials. On the other hand, studies of the hot pressing process and of the influence of porosity (and pore structure) and grain size on thermoelectric energy conversion will be undertaken using  $SiB_6$  as a model material. Dopant studies on  $SiB_6$  will have the aim of increasing the electrical conductivity in order to improve the figure of merit.

V. REFERENCES

1. D. P. Spitzer, J. Phys. Chem. Solids, 31 (1970) 19.
2. G. A. Slack, Solid State Physics, 34 (1979) 1.
3. K. A. Mason and G. Muller-Vogt, J. Crystal Growth, 63 (1983) 34.
4. Y. Sasaki, S. Asanabe and D. Shinoda, U. S. Pat 3,072,733 (Jan 8, 1963).
5. W. B. Bienert and F. M. Gillen, U. S. Pat 3,407,037 (Oct. 22, 1968).
6. D. E. Hill and A. Epstein, U. S. Pat 3,138,486 (June 23, 1964).
7. J. Rasneur and C. Cauchemont, C. R. Acad. Sci. Paris, 286 (1978) C589.
8. J. Rasneur and F. Marion, C. R. Acad. Sci. Paris, 288 (1979) C185.
9. L. M. Litz and J. M. Blocher in "High Temperature Materials and Technology," (Ed. I. E. Campbell and E. M. Sherwood) Wiley, NY, 1967.
10. G. V. Samsonov and I. M. Vinitiskii, Handbook of Refractory Compounds, Plenum, NY, 1980.
11. J. Flahaut in Handbook on the Physics and Chemistry of the Rare Earths (Ed. K. A. G. Schneider and L. Eyring), N. Holland, 1979.
12. A. V. Golubkov et al, Physical Properties of the Chalcogenides of Rare Earth Elements, DOE-tr-6, (1973).
13. M. D. Houston, U. S. Pat 3,009,977 (Nov. 21, 1961).
14. H. C. Longuet-Higgins and M. de V. Roberts, Proc. Roy Soc. London, A224 (1954) 336.
15. Y. B. Paderno and G. V. Samsonov, Dokl. Akad. Nauk SSSR, 137 (1960) 646.
16. R. W. Johnson and A. H. Daane, J. Chem. Phys. 38 (1963) 425.
17. G. A. Slack, D. W. Oliver, G. D. Brower and J. D. Young, J. Phys. Chem. Solids, 38 (1977) 45.
18. K. Spear in
19. W. Harrison, Phys. Rev., B24 (1981) 5835.

20. W. A. Harrison, Phys. Rev., B27 (2983) 3592.
21. H. C. Longuet-Higgins and M. de V. Roberts, Proc. Roy Soc. London, A230 (1955) 110.
22. G. A. Slack, D. W. Oliver and F. H. Horn, Phys. Rev., B4 (1971) 1714.
23. J. P. Dismukes, L. Ekstrom, E. F. Staggmeier, I. Kudman, and D. S. Beers, J. Appl. Phys., 35 (1964) 2899.
24. R. Berman, Thermal Conduction in Solids, Clarendon Press, Oxford, 1975.
25. B. A. Auld, Wave Motion, 1 (1979) 3.
26. B. A. Auld, S. Ayter, and M. Tan, 1978 IEEE Ultrasonics Symposium Proceedings, IEEE Catalogue Number 78CH 1344-1SU.
27. L. Brillouin, Wave Propagation in Periodic Structures, McGraw-Hill, New York, 1946.
28. B. Pistoulet, J. C. Robert, J. M. Dusseau, F. M. Roche and P. Girard, Inst. Phys. Conf. Ser., 43 (1979) 793.
29. J. L. Hoard, D. B. Sullenger, C. H. L. Kennard and R. E. Hughes, J. Sol. St. Chem. 1 (1970) 268.
30. T. Lundstrom and L. E. Tergenius, J. Less-Comm. Met., 47 (1976) 23.
31. M. Vlasse and J. C. Viala, J. Sol. St. Chem., 37 (1981) 181.
32. J. Rosolowski, Proc. 1982 Working Group on Thermoelectrics, JPL, Dec. 7-9, 1982, p. 441.
33. J. F. Goff and J. R. Lowney, Proc. 1st Conf. on Thermoelectric Energy Conv., Arlington, TX, 1976, p. 47.
34. R. P. Chasmar and R. Stratton, J. Electron Control 7 (1959) 52.
35. O. A. Golikova, A. A. Berezin, V. K. Zaitsev, M. M. Kazanin, V. M. Orlov, L. S. Stalibus and E. N. Tkalenko, J. Less. Comm. Met., 47 (1976) 129.
36. O. A. Golikova, Phys. Stat. Sol. (a) 51 (1979) 11.
37. D. Zoltan, Proc. 1982 Working Group on Thermoelectrics, Dec. 7-9, 1982, p. 245.

38. N. Z. Lupu, N. M. Tallan and D. S. Tannhauser, *Rev. Sci. Instrum.*, 38 (1967) 1658.
39. H. L. McKinzie and D. S. Tannhauser, *J. Appl. Phys.* 40 (1969) 4954.
40. D. Elwell and D. S. Tannhauser, *Solid State Comm.* 8(1970) 179.
41. R. H. Friend and N. Bett, *J. Phys. E.*, 13 (1980) 294.
42. R. F. Giese, J. Economy and V. I. Matkovich, *Zeit. Krist.*, 122 (1965) 144.
43. C. F. Cline, *J. Electrochem. Soc.*, 106 (1959) 322.
44. H. Nowotny, E. Piegger, R. Kiffer and F. Benesovsky, *Monats. fur Chemie*, 89 (1958) 611.
45. G. Malé and D. Salanoubat, *Rev. int. haut. temp. refract.*, 18 (1981) 109.
46. E. A. Dzhafarov, O. A. Golikova and M. I. Aliev, *Dokl. Akad. Nauk. AzSSSR*, 36 (1980) 23.
47. R. P. Elliot, *Structure of Binary Alloys*, Metallurgia (1970).
48. J. C. Viala and J. Bouix, *J. Less Comm. Met.*, 71 (1980) 195.
49. A. Sher, D. Ilzyer and M. Shiloh, *Proc. 4th Intl. Conf. on Thermoelectric Energy Conv.*, U. Texas Arlington, March 10-12, 1982, p. 35.
50. R. S. Feigelson and W. D. Kingery, *Special Ceramics 1962* (Academic Press, London) p. 27.
51. M. Bouchacourt and F. Thevenot, *Mat. Res. Bull.* 17 (1982) 1353.
52. C. Wood, *JPI Report*, D-302 (October 1982).